

1      **Global inorganic nitrate production mechanisms:**

2      **Comparison of a global model with nitrate isotope**

3      **observations**

4

5      Becky Alexander<sup>1</sup>, Tomás Sherwen<sup>2,3</sup>, Christopher D. Holmes<sup>4</sup>, Jenny A. Fisher<sup>5</sup>, Qianjie  
6      Chen<sup>1,6</sup>, Mat J. Evans<sup>2,3</sup>, Prasad Kasibhatla<sup>7</sup>

7

8      <sup>1</sup>Department of Atmospheric Sciences, University of Washington, Seattle, WA 98195, USA

9      <sup>2</sup>Wolfson Atmospheric Chemistry Laboratories, Department of Chemistry, University of York, York YO10 5DD, UK

10     <sup>3</sup>National Center for Atmospheric Science, University of York, York YO10 5DD, UK

11     <sup>4</sup>Department of Earth, Ocean and Atmospheric Science, Florida State University, Tallahassee, FL 32306, USA

12     <sup>5</sup>Centre for Atmospheric Chemistry, University of Wollongong, Wollongong, New South Wales 2522, Australia

13     <sup>6</sup>Now at Department of Chemistry, University of Michigan, Ann Arbor, MI 48109, USA

14     <sup>7</sup>Nicholas School of the Environment, Duke University, Durham, NC 27708, USA

15

16     Correspondence to: Becky Alexander ([beckya@uw.edu](mailto:beckya@uw.edu))

17

18     **Abstract.** The formation of inorganic nitrate is the main sink for nitrogen oxides ( $\text{NO}_x = \text{NO} + \text{NO}_2$ ). Due to the  
19     importance of  $\text{NO}_x$  for the formation of tropospheric oxidants such as the hydroxyl radical ( $\text{OH}$ ) and ozone,  
20     understanding the mechanisms and rates of nitrate formation is paramount for our ability to predict the atmospheric  
21     lifetimes of most reduced trace gases in the atmosphere. The oxygen isotopic composition of nitrate ( $\Delta^{17}\text{O}(\text{nitrate})$ ) is  
22     determined by the relative importance of  $\text{NO}_x$  sinks, and thus can provide an observational constraint for  $\text{NO}_x$   
23     chemistry. Until recently, the ability to utilize  $\Delta^{17}\text{O}(\text{nitrate})$  observations for this purpose was hindered by our lack  
24     of knowledge about the oxygen isotopic composition of ozone ( $\Delta^{17}\text{O}(\text{O}_3)$ ). Recent and spatially widespread  
25     observations of  $\Delta^{17}\text{O}(\text{O}_3)$ , and motivate an updated comparison of modeled and observed  $\Delta^{17}\text{O}(\text{nitrate})$  and a

1 reassessment of modeled nitrate formation pathways. Model updates based on recent laboratory studies of  
2 heterogeneous reactions renders dinitrogen pentoxide ( $\text{N}_2\text{O}_5$ ) hydrolysis as important as  $\text{NO}_2 + \text{OH}$  (both 41%) for  
3 global inorganic nitrate production near the surface (below 1 km altitude). All other nitrate production mechanisms  
4 individually represent less than 6% of global nitrate production near the surface, but can be dominant locally. Updated  
5 reaction rates for aerosol uptake of  $\text{NO}_2$  result in significant reduction of nitrate and nitrous acid (HONO) formed  
6 through this pathway in the model, and render  $\text{NO}_2$  hydrolysis a negligible pathway for nitrate formation globally.  
7 Although photolysis of aerosol nitrate may have implications for  $\text{NO}_x$ , HONO and oxidant abundances, it does not  
8 significantly impact the relative importance of nitrate formation pathways. Modeled  $\Delta^{17}\text{O}(\text{nitrate})$  ( $28.6 \pm 4.5\text{\textperthousand}$ )  
9 compares well with the average of a global compilation of observations ( $27.6 \pm 5.0\text{\textperthousand}$ ) when assuming  $\Delta^{17}\text{O}(\text{O}_3) =$   
10  $26\text{\textperthousand}$ , giving confidence in the model's representation of the relative importance of ozone versus  $\text{HO}_x$  ( $= \text{OH} + \text{HO}_2$   
11  $+ \text{RO}_2$ ) in  $\text{NO}_x$  cycling and nitrate formation on the global scale.

12

## 13 1. Introduction

14

15 Nitrogen oxides ( $\text{NO}_x = \text{NO} + \text{NO}_2$ ) are a critical ingredient for the formation of tropospheric ozone ( $\text{O}_3$ ).  
16 Tropospheric ozone is a greenhouse gas, is a major precursor for the hydroxyl radical ( $\text{OH}$ ), and is considered an air  
17 pollutant due to its negative impacts on human health. The atmospheric lifetime of  $\text{NO}_x$  is determined by its oxidation  
18 to inorganic and organic nitrate. The formation of inorganic nitrate ( $\text{HNO}_3(\text{g})$  and particulate  $\text{NO}_3^-$ ) is the dominant  
19 sink for  $\text{NO}_x$  globally, while formation of organic nitrate may be significant in rural and remote continental locations  
20 (Browne and Cohen, 2014). Organic nitrate as a sink for  $\text{NO}_x$  may be becoming more important in regions in North  
21 America and Europe where  $\text{NO}_x$  emissions have declined (Zare et al., 2018). Uncertainties in the rate of oxidation of  
22  $\text{NO}_x$  to nitrate has been shown to represent a significant source of uncertainty for ozone and  $\text{OH}$  formation in models  
23 (e.g., Newsome and Evans (2017)) , with implications for our understanding of the atmospheric lifetime of species  
24 such as methane, whose main sink is reaction with  $\text{OH}$ .

25

26  $\text{NO}_x$  is emitted to the atmosphere primarily as NO by fossil fuel and biomass/biofuel burning, soil microbes, and  
27 lightning. Anthropogenic sources from fossil fuel and biofuel burning and from the application of fertilizers to soil  
28 for agriculture currently dominate  $\text{NO}_x$  sources to the atmosphere (Jaeglé et al., 2005). After emission, NO is rapidly

1 oxidized to  $\text{NO}_2$  by ozone ( $\text{O}_3$ ), peroxy ( $\text{HO}_2$ ) and hydroperoxy radicals ( $\text{RO}_2$ ), and halogen oxides (e.g.,  $\text{BrO}$ ). During  
2 the daytime,  $\text{NO}_2$  is rapidly photolyzed to  $\text{NO} + \text{O}$  at wavelengths ( $\lambda$ )  $< 398$  nm.  $\text{NO}_x$  cycling between  $\text{NO}$  and  $\text{NO}_2$   
3 proceeds several orders of magnitude faster than oxidation of  $\text{NO}_x$  to nitrate during the daytime (Michalski et al.,  
4 2003).

5  
6 Formation of inorganic nitrate is dominated by oxidation of  $\text{NO}_2$  by  $\text{OH}$  during the day and by the hydrolysis of  
7 dinitrogen pentoxide ( $\text{N}_2\text{O}_5$ ) at night (Alexander et al., 2009). Recent implementation of reactive halogen chemistry  
8 in models of tropospheric chemistry show that formation of nitrate from the hydrolysis of halogen nitrates ( $\text{XNO}_3$ ,  
9 where  $\text{X} = \text{Br, Cl, or I}$ ) is also a sink for  $\text{NO}_x$  with implications for tropospheric ozone,  $\text{OH}$ , reactive halogens, and  
10 aerosol formation (Schmidt et al., 2016; Sherwen et al., 2016; Saiz-Lopez et al., 2012; Long et al., 2014; Parrella et al.,  
11 2012; von Glasow and Crutzen, 2004; Yang et al., 2005). Other inorganic nitrate formation pathways include  
12 hydrogen-abstraction of hydrocarbons by the nitrate radical ( $\text{NO}_3$ ), heterogeneous reaction of  $\text{N}_2\text{O}_5$  with particulate  
13 chloride ( $\text{Cl}^-$ ), heterogeneous uptake of  $\text{NO}_2$  and  $\text{NO}_3$ , direct oxidation of  $\text{NO}$  to  $\text{HNO}_3$  by  $\text{HO}_2$ , and hydrolysis of  
14 organic nitrate (Atkinson, 2000). Inorganic nitrate partitions between the gas ( $\text{HNO}_3(\text{g})$ ) and particle ( $\text{NO}_3^-$ ) phases,  
15 with its relative partitioning dependent upon aerosol abundance, aerosol liquid water content, aerosol chemical  
16 composition, and temperature. Inorganic nitrate is lost from the atmosphere through wet or dry deposition to the  
17 Earth's surface with a global lifetime against deposition on the order of 3-4 days (Park et al., 2004).

18  
19 Formation of inorganic nitrate was thought to be a permanent sink for  $\text{NO}_x$  in the troposphere due to the slow  
20 photolysis of nitrate compared to deposition. However, laboratory and field studies have shown that  $\text{NO}_3^-$  adsorbed  
21 on surfaces is photolyzed at rates much higher than  $\text{HNO}_3(\text{g})$  (Ye et al., 2016). For example, the photolysis of  $\text{NO}_3^-$   
22 in snow grains on ice sheets has a profound impact on the oxidizing capacity of the polar atmosphere (Domine and  
23 Shepson, 2002). More recently, observations of  $\text{NO}_x$  and nitrous acid (HONO) provide evidence of photolysis of  
24 aerosol  $\text{NO}_3^-$  in the marine (Reed et al., 2017; Ye et al., 2016) and continental (Ye et al., 2018; Chen et al., 2019)  
25 boundary layer, with implications for ozone and  $\text{OH}$  (Kasibhatla et al., 2018).

26  
27 Organic nitrates form during reaction of  $\text{NO}_x$  and  $\text{NO}_3$  with biogenic volatile organic compounds (BVOCs) and their  
28 oxidation products (organic peroxy radicals,  $\text{RO}_2$ ) (Browne and Cohen, 2014; Liang et al., 1998). Products of these

1 reactions include peroxy nitrates ( $\text{RO}_2\text{NO}_2$ ) and alkyl and multifunctional nitrates ( $\text{RONO}_2$ ) (O'Brien et al., 1995).  
2 Peroxy nitrates are thermally unstable and decompose back to  $\text{NO}_x$  on the order of minutes to days at warm  
3 temperatures. Decomposition of longer-lived peroxy nitrates such as peroxyacetyl nitrate (PAN) can provide a source  
4 of  $\text{NO}_x$  to remote environments (Singh et al., 1992). The fate of  $\text{RONO}_2$  is uncertain. First-generation  $\text{RONO}_2$  is  
5 oxidized to form second-generation  $\text{RONO}_2$  species with a lifetime of about a week for the first-generation species  
6 with  $\geq 4$  carbon atoms, and up to several weeks for species with fewer carbon atoms (e.g., days to weeks for methyl  
7 nitrate) (Fisher et al., 2018). Subsequent photolysis and oxidation of second-generation  $\text{RONO}_2$  species can lead to  
8 the recycling of  $\text{NO}_x$  (Müller et al., 2014), although recycling efficiencies are highly uncertain (Horowitz et al.,  
9 2007;Paulot et al., 2009).  $\text{RONO}_2$  can also partition to the particle phase ( $\text{pRONO}_2$ ) contributing to organic aerosol  
10 formation (Xu et al., 2015).  $\text{pRONO}_2$  is removed from the atmosphere by deposition to the surface, or through  
11 hydrolysis to form inorganic nitrate and alcohols (Rindelaub et al., 2015;Jacobs et al., 2014).  
12

13 The oxygen isotopic composition ( $\Delta^{17}\text{O} = \delta^{17}\text{O} - 0.52 \times \delta^{18}\text{O}$ ) of nitrate is determined by the relative importance of  
14 oxidants leading to nitrate formation from the oxidation of  $\text{NO}_x$  (Michalski et al., 2003). Observations of the oxygen  
15 isotopic composition of nitrate ( $\Delta^{17}\text{O}(\text{nitrate})$ ) have been used to quantify the relative importance of different nitrate  
16 formation pathways and to assess model representation of the chemistry of nitrate formation in the present day  
17 (Alexander et al., 2009;Michalski et al., 2003;Costa et al., 2011;Ishino et al., 2017a;Morin et al., 2009;Morin et al.,  
18 2008;Savarino et al., 2007;Kunasek et al., 2008;Savarino et al., 2013;McCabe et al., 2007;Morin et al., 2007;Hastings  
19 et al., 2003;Kaiser et al., 2007;Brothers et al., 2008;Ewing et al., 2007) and in the past from nitrate archived in ice  
20 cores (Sofen et al., 2014;Alexander et al., 2004;Geng et al., 2014;Geng et al., 2017). Ozone-influenced reactions in  
21  $\text{NO}_x$  oxidation lead to high  $\Delta^{17}\text{O}(\text{nitrate})$  values while  $\text{HO}_x$ -influenced reactions lead to  $\Delta^{17}\text{O}(\text{nitrate})$  near zero.  
22 Oxidation by  $\text{XO}$  (where  $\text{X} = \text{Br}$ ,  $\text{Cl}$ , or  $\text{I}$ ) leads to  $\Delta^{17}\text{O}(\text{nitrate})$  values similar to reactions with ozone because the  
23 oxygen atom in  $\text{XO}$  is derived from the reaction  $\text{X} + \text{O}_3$ . Therefore,  $\Delta^{17}\text{O}(\text{nitrate})$  is determined by the relative  
24 importance of  $\text{O}_3 + \text{XO}$  versus  $\text{HO}_x$  ( $= \text{OH} + \text{HO}_2 + \text{RO}_2$ ) in both  $\text{NO}_x$  cycling and oxidation to nitrate. Although  
25 freshly emitted  $\text{NO}$  will have  $\Delta^{17}\text{O}(\text{NO}) = 0\text{\textperthousand}$ ,  $\text{NO}_x$  achieves isotopic equilibrium during the daytime due to rapid  
26  $\text{NO}_x$  cycling, so that its  $\Delta^{17}\text{O}$  value ( $\Delta^{17}\text{O}(\text{NO}_x)$ ) is solely determined by the relative abundance of  $(\text{O}_3 + \text{XO})$  to  $(\text{HO}_2$   
27  $+ \text{RO}_2)$  (Michalski et al., 2003).  
28

1 The  $\Delta^{17}\text{O}$  value of  $\text{HO}_x$  ( $\Delta^{17}\text{O}(\text{HO}_x)$ ) is near zero due to isotopic exchange of OH with water vapor (Dubey et al.,  
2 1997). Previously, observations of the  $\Delta^{17}\text{O}$  value of ozone ( $\Delta^{17}\text{O}(\text{O}_3)$ ) showed a large range (6 – 54‰) (Johnston  
3 and Thiemens, 1997;Krankowsky et al., 1995), in contrast to laboratory and modeling studies suggesting that the range  
4 of  $\Delta^{17}\text{O}(\text{O}_3)$  in the troposphere should be relatively narrow (30-46 ‰) (Morton et al., 1990;Thiemens, 1990). The  
5 large range of observed  $\Delta^{17}\text{O}(\text{O}_3)$  values is thought to be due to sampling artifacts (Brenninkmeijer et al., 2003).  
6 Uncertainty in the value of  $\Delta^{17}\text{O}(\text{O}_3)$  has been the largest source of uncertainty in quantification of nitrate formation  
7 pathways using observations of  $\Delta^{17}\text{O}(\text{nitrate})$  (Alexander et al., 2009). Previous modeling studies showed good  
8 agreement with observations of  $\Delta^{17}\text{O}(\text{nitrate})$  when assuming that the bulk oxygen isotopic composition of ozone  
9 ( $\Delta^{17}\text{O}(\text{O}_3)$ ) is equal to 35‰ (Alexander et al., 2009;Michalski et al., 2003); but varied in their assumption on terminal  
10 oxygen atom versus statistical isotopic transfer from  $\text{O}_3$  to the reactant (NO and  $\text{NO}_2$ ). This is an important distinction  
11 because it is now known that the  $^{17}\text{O}$  enrichment in  $\text{O}_3$  is contained entirely in its terminal oxygen atoms, and it is the  
12 terminal oxygen atom that is transferred from  $\text{O}_3$  (Vicars et al., 2012;Berhanu et al., 2012;Bhattacharya et al.,  
13 2008;Savarino et al., 2008;Michalski and Bhattacharya, 2009;Bhattacharya et al., 2014), so that the  $\Delta^{17}\text{O}$  value of the  
14 oxygen atom transferred from ozone to the product is 50% larger than the bulk  $\Delta^{17}\text{O}(\text{O}_3)$  value. Recently, much more  
15 extensive observations of  $\Delta^{17}\text{O}(\text{O}_3)$  using a new technique (Vicars et al., 2012) consistently show  $\Delta^{17}\text{O}(\text{O}_3) = 26 \pm$   
16 1‰ in diverse locations (Vicars et al., 2012;Ishino et al., 2017b;Vicars and Savarino, 2014), and suggest that previous  
17 modeling studies are biased low in  $\Delta^{17}\text{O}(\text{nitrate})$  (e.g., Alexander et al. (2009)), which would occur if the model  
18 underestimated the relative role of ozone in  $\text{NO}_x$  chemistry. These new observations of  $\Delta^{17}\text{O}(\text{O}_3)$ , combined with  
19 improved understanding and hence more comprehensive chemical representation of nitrate formation in models,  
20 motivates an updated comparison of observed and modeled  $\Delta^{17}\text{O}(\text{nitrate})$  as an observational constraint for the relative  
21 importance of nitrate formation pathways in the atmosphere. Note that laboratory studies show that the magnitude of  
22  $\Delta^{17}\text{O}(\text{O}_3)$  is dependent on temperature and pressure (Heidenreich and Thiemens, 1986;Thiemens, 1990;Morton et al.,  
23 1990). The observations of  $\Delta^{17}\text{O}(\text{O}_3)$  by Vicars et al. (2012, 2013) were at the surface over a large temperature range,  
24 but may not reflect the value of  $\Delta^{17}\text{O}(\text{O}_3)$  at higher altitudes. However, with the exception of lightning, whose  
25 emissions are presently several times smaller than  $\text{NO}_x$  emissions from anthropogenic and biomass burning sources  
26 (Murray, 2016),  $\text{NO}_x$  sources emit at the surface. With a  $\text{NO}_x$  lifetime relative to its conversion to nitrate on the order  
27 of one day (Levy et al., 1999), most nitrate formation also occurs near the surface. Here, we examine the relative

1 contribution of each nitrate formation pathway in a global chemical transport model and compare the model with  
2 surface observations of  $\Delta^{17}\text{O}(\text{nitrate})$  from around the world.

3

4 **2. Methods**

5

6 We use the GEOS-Chem global chemical transport model version 12.0.0 driven by assimilated meteorology from the  
7 MERRA-2 reanalysis product with a native resolution of  $0.5^\circ \times 0.625^\circ$  and 72 vertical levels from the surface up to  
8 the 0.01 hPa pressure level. For computational expediency, the horizontal and vertical resolution were downgraded  
9 to  $4^\circ \times 5^\circ$  and 47 vertical levels. GEOS-Chem was originally described in Bey et al. (2001) and includes coupled  
10  $\text{HO}_x\text{-NO}_x\text{-VOC}$ -ozone-halogen-aerosol tropospheric chemistry as described in Sherwen et al. (2016) and Sherwen et  
11 al. (2017) and organic nitrate chemistry as described in Fisher et al. (2016). Aerosols interact with gas-phase chemistry  
12 through the effect of aerosol extinction on photolysis rates (Martin et al., 2003) and heterogeneous chemistry (Jacob,  
13 2000). The model calculates deposition for both gas species and aerosols (Liu et al., 2001; Zhang et al., 2001; Wang  
14 et al., 1998).

15

16 Global anthropogenic emissions, including  $\text{NO}_x$ , are from the Community Emissions Data System (CEDS) inventory  
17 from 1950 – 2014 C.E. (Hoesly et al., 2018a). The CEDS global emissions inventory is overwritten by regional  
18 anthropogenic emissions inventories in the U.S. (EPA/NE11), Canada (CAC), Europe (EMEP), and Asia (MIX (Li et  
19 al., 2017)). Global shipping emissions are from the International Comprehensive Ocean-Atmosphere Data Set  
20 (ICOADS), which was implemented into GEOS-Chem as described in Lee et al. (2011).  $\text{NO}_x$  emissions from ships  
21 are processed using the PARANOX module described in Vinken et al. (2011) and Holmes et al. (2014) to account for  
22 non-linear, in-plume ozone and  $\text{HNO}_3$  production. Lightning  $\text{NO}_x$  emissions match the OTD/LIS satellite  
23 climatological observations of lightning flashes as described by Murray et al. (2012). Emissions from open fires are  
24 from the Global Fire Emissions Database (GFED4.1). Biogenic soil  $\text{NO}_x$  emissions are described in Hudman et al.  
25 (2012). Aircraft emissions are from the Aviation Emissions Inventory Code (AEIC) (Stettler et al., 2011).

26

27 Chemical processes leading to nitrate formation in GEOS-Chem have expanded since the previous work of Alexander  
28 et al. (2009). Figure 1 summarizes the formation of inorganic nitrate in the current model. In the model,  $\text{NO}$  is

1 oxidized by  $O_3$ ,  $HO_2$ ,  $RO_2$  and halogen oxides ( $XO = BrO$ ,  $ClO$ ,  $IO$ , and  $OIO$ ) to form  $NO_2$ . The reaction of  $NO +$   
2  $HO_2$  can also form  $HNO_3$  directly, although the branching ratio for this pathway is  $< 1\%$  (Butkovskaya et al., 2005).  
3  $NO_2$  can form  $HNO_3$  directly from its reaction with  $OH$  and through hydrolysis on aerosol surfaces.  $NO_2$  can react  
4 with  $XO$  to form halogen nitrates ( $BrNO_3$ ,  $ClNO_3$ , and  $INO_3$ ), which can then form  $HNO_3$  upon hydrolysis (as  
5 described in Sherwen et al. (2016)).  $NO_2$  can also react with  $O_3$  to form  $NO_3$ , which can then react with  $NO_2$ ,  
6 hydrocarbons (HC), and the biogenic VOCs monoterpenes (MTN) and isoprene (ISOP). Reaction of  $NO_3$  with  $NO_2$   
7 forms  $N_2O_5$ , which can subsequently hydrolyze or react with  $Cl^-$  in aerosol to form  $HNO_3$ . Reaction of  $NO_3$  with HC  
8 forms  $HNO_3$  via hydrogen abstraction. Reactions of  $NO_3$  are only important at night due to its short lifetime against  
9 photolysis. Formation of organic nitrate ( $RONO_2$ ) was recently updated in the model as described in Fisher et al.  
10 (2016). Reaction of  $NO_3$  with MTN and ISOP can form  $RONO_2$ .  $RONO_2$  also forms from the reaction of  $NO$  with  
11  $RO_2$  derived from  $OH$  oxidation of BVOCs.  $RONO_2$  hydrolyzes to form  $HNO_3$  on a timescale of 1 hour. Inorganic  
12 nitrate partitions between the gas ( $HNO_3(g)$ ) and particle ( $NO_3^-$ ) phase according to local thermodynamic equilibrium  
13 as calculated in the ISORROPIA-II aerosol thermodynamic module (Fountoukis and Nenes, 2007).  $HNO_3(g)$  and  
14  $NO_3^-$  are mainly lost from the atmosphere via wet and dry deposition to the surface.

15

16 In the “standard” model, hydrolysis of  $N_2O_5$ ,  $NO_3$  ( $\gamma_{NO_3} = 1 \times 10^{-3}$ ), and  $NO_2$  ( $\gamma_{NO_2} = 1 \times 10^{-4}$ ) occur on aerosol surfaces  
17 only. Uptake and hydrolysis of  $N_2O_5$  on aerosol surfaces depends on the chemical composition of aerosols,  
18 temperature, and humidity as described in Evans and Jacob (2005). Recently, Holmes et al. (2019) updated the  
19 reaction probabilities of the  $NO_2$  and  $NO_3$  heterogeneous reactions in the model to depend on aerosol chemical  
20 composition and relative humidity. Holmes et al. (2019) also updated the  $N_2O_5$  reaction probability to additionally  
21 depend on the  $H_2O$  and  $NO_3^-$  concentrations in aerosol (Bertram and Thornton, 2009). In addition to these updates  
22 for hydrolysis on aerosol, Holmes et al. (2019) included the uptake and hydrolysis of  $N_2O_5$ ,  $NO_2$ , and  $NO_3$  in cloud  
23 water and ice limited by cloud entrainment rates. We incorporate these updates from Holmes et al. (2019) into the  
24 “cloud chemistry” model to examine the impacts on global nitrate production mechanisms. We consider the “cloud  
25 chemistry” model as state-of-the science, and as such we focus on the results of this particular simulation. Additional  
26 model sensitivity studies are also performed and examined relative to the “standard” model simulation, which  
27 represents a more common representation of nitrate chemistry in atmospheric chemistry models. These additional  
28 sensitivity simulations are described in Section 4.

1  
2  $\Delta^{17}\text{O}(\text{nitrate})$  is calculated in the model using monthly-mean, local chemical production rates, rather than by treating  
3 different isotopic combinations of nitrate as separate tracers that can be transported in the model. Alexander et al.  
4 (2009) transported four nitrate tracers, one each for nitrate production by  $\text{NO}_2 + \text{OH}$ ,  $\text{N}_2\text{O}_5$  hydrolysis,  $\text{NO}_3 + \text{HC}$ , and  
5 nitrate originating from its formation in the stratosphere. Since  $\Delta^{17}\text{O}(\text{NO}_x)$  was not transported in the Alexander et al.  
6 (2009) model, it was calculated using local production rates, so effectively only one-third of the  $\Delta^{17}\text{O}(\text{nitrate})$  was  
7 transported in Alexander et al. (2009). Accurately accounting for transport of  $\Delta^{17}\text{O}(\text{nitrate})$  in the model would require  
8 transporting all individual isotopic combinations of the primary reactant (NO), the final product (nitrate), and each  
9 reaction intermediate (e.g.,  $\text{N}_2\text{O}_5$ ), which we do not do here due to the large computational costs. Thus, the model  
10 results shown here represent  $\Delta^{17}\text{O}(\text{nitrate})$  from local  $\text{NO}_x$  cycling and nitrate production. This may lead to model  
11 biases, particularly in remote regions such as polar-regions in winter-time when most nitrate is likely transported from  
12 lower latitudes or the stratosphere. This should make less difference in polluted regions where most nitrate is formed  
13 locally, or for example in polar regions in summer when photochemical recycling of nitrate in the snowpack represents  
14 a significant local source of  $\text{NO}_x$  at the surface (Domine and Shepson, 2002). Although lack of transport of the isotope  
15 tracers adds uncertainty to direct comparison of the model with observations at any particular location, this approach  
16 will reflect the full range of possible modeled  $\Delta^{17}\text{O}(\text{nitrate})$  values for the current chemical mechanism, which can  
17 then be compared to the range of observed  $\Delta^{17}\text{O}(\text{nitrate})$  values around the globe.  
18

19 The  $\Delta^{17}\text{O}(\text{nitrate})$  value of nitrate produced from each production pathway is calculated as shown in Table 1. The  
20 value of  $A$  in Table 1 represents the relative importance of the oxidation pathways of NO to  $\text{NO}_2$  where the oxygen  
21 atom transferred comes from ozone ( $\text{NO} + \text{O}_3$  and  $\text{NO} + \text{XO}$ ):

$$22 A = \frac{k_{\text{O}_3 + \text{NO}}[\text{O}_3] + k_{\text{XO} + \text{NO}}[\text{XO}]}{k_{\text{O}_3 + \text{NO}}[\text{O}_3] + k_{\text{XO} + \text{NO}}[\text{XO}] + k_{\text{HO}_2 + \text{NO}}[\text{HO}_2] + k_{\text{RO}_2 + \text{NO}}[\text{RO}_2]} \quad (\text{E1})$$

23 In E1,  $k$  represents the local reaction rate constant for each of the four reactions,  $\text{XO} = \text{BrO}$ ,  $\text{ClO}$ ,  $\text{IO}$ , and  $\text{OIO}$ , and  
24 we assume  $\Delta^{17}\text{O}(\text{XO})$  is equal to the  $\Delta^{17}\text{O}$  value of the terminal oxygen atoms of ozone, as described in more detail  
25 below. This effectively assumes that the other oxidation pathways ( $\text{NO} + \text{HO}_2$  and  $\text{NO} + \text{RO}_2$ ) yield  $\Delta^{17}\text{O}(\text{NO}_x) =$   
26 0‰. Although  $\text{HO}_2$  may have a small  $^{17}\text{O}$  enrichment on the order of 1-2‰ (Savarino and Thiemens, 1999b), the  
27 assumption that this pathway yields  $\Delta^{17}\text{O}(\text{NO}_x) = 0\text{‰}$  simplifies the calculation and leads to negligible differences in

1 calculated  $\Delta^{17}\text{O}$ (nitrate) (Michalski et al., 2003). This approach assumes that  $\text{NO}_x$  cycling is in photochemical steady-  
2 state, which only occurs during the daytime.  $A$  is calculated in the model as the 24-hour average  $\text{NO}_2$  production rate,  
3 rather than the daytime average only. As was shown in Alexander et al. (2009), rapid daytime  $\text{NO}_x$  cycling dominates  
4 the calculated 24-hour averaged  $A$  value, leading to negligible differences in calculated  $\Delta^{17}\text{O}$ (nitrate) for 24-hour  
5 averaged values versus daytime averaged values.

6

7  $\text{NO}_x$  formed during the day will retain its daytime  $\Delta^{17}\text{O}(\text{NO}_x)$  signature throughout the night due to lack of  $\text{NO}_2$   
8 photolysis (Morin et al., 2011), suggesting similar  $A$  values for the nighttime reactions (R2, R4, R5, R8, and R10 in  
9 Table 1). However, NO emitted at night will not undergo photochemical recycling; initially suggesting that NO will  
10 retain its emitted  $\Delta^{17}\text{O}(\text{NO})$  value of 0‰ prior to sunrise. Thus, any NO emitted at night and oxidized to  $\text{NO}_2$  before  
11 sunrise will result in  $\Delta^{17}\text{O}(\text{NO}_2)$  equal to one-half of the  $\Delta^{17}\text{O}$  value of the oxidant, since only one of the two oxygen  
12 atoms of  $\text{NO}_2$  will originate from the oxidant. Since  $\text{HO}_x$  abundance is low at night, ozone will be the dominant  
13 oxidant. Thus, NO both emitted and oxidized to  $\text{NO}_2$  at night will lead to  $A_{night} = 0.5$  (half of the O atoms of  $\text{NO}_2$   
14 originate from  $\text{O}_3$ ). Although isotopic exchange between  $\text{NO} + \text{NO}_2$  (Sharma et al., 1970) and  $\text{NO}_2$  and  $\text{NO}_3$  via  
15 thermal dissociation of  $\text{N}_2\text{O}_5$  (Connell and Johnston, 1979) will tend to increase  $\Delta^{17}\text{O}(\text{NO})$  above its emitted value of  
16 0‰, the bulk  $\Delta^{17}\text{O}$  value of  $\text{NO}_x$  plus  $\text{NO}_3$  system will be lower at night than during the daytime due to the absence  
17 of photochemical cycling at night (Michalski et al., 2014; Morin et al., 2011). Since the atmospheric lifetime of  $\text{NO}_x$   
18 near the surface against nighttime oxidation to nitrate (R2+R4+R5) is typically greater than 24 hours (Figure S1),  
19 most nitrate formed during the nighttime will form from  $\text{NO}_x$  that reached photochemical equilibrium during the  
20 previous day. Thus, we use values of  $A$  calculated as the 24-hour average  $\text{NO}_2$  production rate for calculating the  
21  $\Delta^{17}\text{O}$ (nitrate) value of all nitrate production pathways, including those that can occur at night. Using 24-hour averaged  
22  $A$  values may lead to an overestimate of  $\Delta^{17}\text{O}$ (nitrate) in locations with more rapid nighttime nitrate formation rates  
23 such as in China and India (Figure S1). However, even in these locations the lifetime of  $\text{NO}_x$  against nighttime  
24 oxidation is greater than 12 hours, suggesting that over half of nitrate formation at night occurs from the oxidation of  
25  $\text{NO}_x$  that reached photochemical equilibrium during the daytime. When comparing modeled  $\Delta^{17}\text{O}$ (nitrate) with  
26 observations, we add error bars to model values in these locations (Beijing and Mt. Lulin, Taiwan) that reflect the  
27 range of possible  $A$  values for nighttime nitrate formation, with the high end ( $A_{high}$ ) reflecting 24-hour average  $A$  values

1 and the low end assuming that half of nitrate formation occurs from oxidation of  $\text{NO}_x$  that reached photochemical  
2 equilibrium during the daytime ( $A_{low} = 0.5A + 0.5A_{night}$ , where  $A_{night} = 0.5$ ).

3  
4  $\Delta^{17}\text{O}(\text{nitrate})$  for total nitrate is calculated in the model according to:

5 
$$\Delta^{17}\text{O}(\text{nitrate}) = \sum_{R=R1}^{R10} f_R \Delta^{17}\text{O}(\text{nitrate})_R \quad (\text{E2})$$

6 where  $f_R$  represents the fractional importance of each nitrate production pathway (R1-R10 in Table 1) relative to total  
7 nitrate production, and  $\Delta^{17}\text{O}(\text{nitrate})_R$  is the  $\Delta^{17}\text{O}(\text{nitrate})$  value for each reaction as described in Table 1. To calculate  
8  $\Delta^{17}\text{O}(\text{nitrate})$ , we assume that the mean  $\Delta^{17}\text{O}$  value of the ozone molecule ( $\Delta^{17}\text{O}(\text{O}_3)$ ) is equal to 26‰ based on recent  
9 observations (Vicars et al., 2012; Ishino et al., 2017b; Vicars and Savarino, 2014), and that it is the terminal oxygen  
10 atom that are transferred to the oxidation product during chemical reactions (Savarino et al., 2008; Berhanu et al.,  
11 2012). Thus, we assume that the  $\Delta^{17}\text{O}$  value of the oxygen atom transferred from  $\text{O}_3$  ( $\Delta^{17}\text{O}(\text{O}_3^*)$ ) =  $1.5 \times \Delta^{17}\text{O}(\text{O}_3)$ ,  
12 as in previous work (e.g., (Morin et al., 2011)), where  $\Delta^{17}\text{O}(\text{O}_3^*)$  represents the  $\Delta^{17}\text{O}$  value of the terminal oxygen  
13 atoms in ozone. Assuming that  $\Delta^{17}\text{O}(\text{O}_3) = 26\text{\textperthousand}$  based on recent observations, this leads to  $\Delta^{17}\text{O}(\text{O}_3^*) = 39\text{\textperthousand}$ .

14  
15  
16 **3. Results and Discussion**  
17

18 Figure 1 shows the relative importance of the different oxidation pathways of  $\text{NO}$  to  $\text{NO}_2$  and nitrate formation below  
19 1 km altitude in the model for the “cloud chemistry” simulation, with equivalent values for the “standard” simulation  
20 shown in parentheses. We focus on model results near the surface (below 1 km) because these can be compared to  
21 observations; currently only surface observations of  $\Delta^{17}\text{O}(\text{nitrate})$  are available. We note that two observation data  
22 sets (from Bermuda (Hastings et al., 2003) and Princeton, NJ (Kaiser et al., 2007)) are rainwater samples and thus  
23 may represent nitrate formed aloft. However, since cloud water peaks on average near 1 km altitude in the MERRA2  
24 meteorology used to drive GEOS-Chem, our model sampling strategy should capture the majority of the influence of  
25 clouds on the chemistry of nitrate formation. The dominant oxidant of  $\text{NO}$  to  $\text{NO}_2$  is  $\text{O}_3$  (84-85%). Much of the  
26 remaining oxidation occurs due to the reaction with peroxy radicals ( $\text{HO}_2$  and  $\text{RO}_2$ ). Oxidation of  $\text{NO}$  to  $\text{NO}_2$  by  $\text{XO}$   
27 is minor (1%) and occurs over the oceans because the main source of tropospheric reactive halogens is from sea salt

1 aerosol and sea water (Chen et al., 2017; Sherwen et al., 2016; Wang et al., 2018) (Figure 2). In the model, the global,  
2 annual mean lifetime of  $\text{NO}_x$  in the troposphere against oxidation to nitrate is about 1 day; about 50% of this loss is  
3 from the reaction of  $\text{NO}_2 + \text{OH}$ .  $\text{NO}_x$  loss from  $\text{N}_2\text{O}_5$  becomes more important near the surface where aerosol surface  
4 area is relatively high. The global, annual mean lifetime of nitrate in the troposphere against wet and dry deposition  
5 to the surface is about 3 days.

6

7 For both the “cloud chemistry” and “standard” simulations, the two most important nitrate formation pathways are  
8  $\text{NO}_2 + \text{OH}$  (41-42%) and  $\text{N}_2\text{O}_5$  hydrolysis (28-41%) , the latter of which is dominant over the mid- to high-northern  
9 continental latitudes during winter where both  $\text{NO}_x$  emissions and aerosol abundances are relatively large (Figures 1  
10 and 3). The “cloud chemistry” simulation results in an equal importance of nitrate formation via  $\text{NO}_2 + \text{OH}$  and  $\text{N}_2\text{O}_5$   
11 hydrolysis (both 41%) due to increases in the rate of  $\text{N}_2\text{O}_5$  uptake in clouds and decreases in the importance of  $\text{NO}_2$   
12 hydrolysis, which can compete with  $\text{N}_2\text{O}_5$  formation at night. In the “standard” model,  $\text{NO}_2$  hydrolysis represents an  
13 important nitrate production mechanism (12%), but it is negligible in the “cloud chemistry” simulation due to the  
14 reduction in the reaction probability (from  $\gamma_{\text{NO}_2} = 10^{-4}$  to  $\gamma_{\text{NO}_2} = 10^{-4}$  to  $10^{-8}$ ) in the model, which is supported by  
15 laboratory studies (Burkholder et al., 2015; Crowley et al., 2010; Tan et al., 2016). The formation of  $\text{HNO}_3$  from the  
16 hydrolysis of  $\text{RONO}_2$  formed from both daytime ( $\text{NO} + \text{RO}_2$ ) and nighttime ( $\text{NO}_3 + \text{MTN/ISOP}$ ) reactions represents  
17 6% of total, global nitrate formation (Figure 1) and is dominant over Amazonia (Figure 3).  $\text{RONO}_2$  hydrolysis  
18 represents up to 20% of inorganic nitrate formation in the southeast U.S. (Figure 3). This is similar to Fisher et al.  
19 (2016) who estimated that formation of  $\text{RONO}_2$  accounts for up to 20% of  $\text{NO}_x$  loss in this region during summer,  
20 with  $\text{RONO}_2$  hydrolysis representing 60% of  $\text{RONO}_2$  loss. Globally, the formation of inorganic nitrate from the  
21 hydrolysis of  $\text{RONO}_2$  is dominated by  $\text{RONO}_2$  formation from the daytime reactions (3-6%), while the formation of  
22  $\text{RONO}_2$  from nighttime reactions represents up to 3%. The relative importance of nighttime and daytime  $\text{RONO}_2$   
23 formation is expressed as a range because precursors to  $\text{RONO}_2$  that formed from monoterpenes can form from both  
24 daytime and nighttime reactions, and these precursors are not separately diagnosed in the model output.  $\text{HNO}_3$   
25 formation from  $\text{NO}_3 + \text{HC}$  and the hydrolysis of  $\text{XNO}_3$  are small globally (5-6%). Although  $\text{XNO}_3$  hydrolysis is the  
26 dominant nitrate formation pathway over the remote oceans (Figure 3), its contribution to total, global nitrate  
27 production is relatively small due to small local  $\text{NO}_x$  sources in these regions.

1

2 Figures 4 - 6 show modeled  $\Delta^{17}\text{O}(\text{nitrate})$  for the “cloud chemistry” simulation (the “standard” simulation is shown in  
3 Figures S2 – S4). Figure 4 shows modeled annual-mean  $\Delta^{17}\text{O}(\text{nitrate})$  below 1 km altitude ( $\Delta^{17}\text{O}(\text{NO}_2)$  is shown in  
4 Figure S5). The model predicts an annual-mean range of  $\Delta^{17}\text{O}(\text{nitrate}) = 4 - 33\text{\textperthousand}$  near the surface. The lowest values  
5 are over Amazonia due to the dominance of  $\text{RONO}_2$  hydrolysis and the highest values are over the mid-latitude oceans  
6 due to the dominance of  $\text{XNO}_3$  hydrolysis (Figures 3 and 4).

7

8 Figure 5 compares the model with a global compilation of  $\Delta^{17}\text{O}(\text{nitrate})$  observations from around the world.  
9 Observations included in Figure 5 include locations where there is enough data to calculate monthly means (McCabe  
10 et al., 2006;Kunasek et al., 2008;Hastings et al., 2003;Kaiser et al., 2007;Michalski et al., 2003;Guha et al.,  
11 2017;Savarino et al., 2013;Ishino et al., 2017b;Savarino et al., 2007;Alexander et al., 2009;He et al., 2018b;Fibiger et  
12 al., 2013;Wang et al., 2014). Figure 6 compares the seasonality in modeled  $\Delta^{17}\text{O}(\text{nitrate})$  to the observations where  
13 samples were collected over the course of approximately one year (McCabe et al., 2006;Kunasek et al., 2008;Kaiser  
14 et al., 2007;Michalski et al., 2003;Guha et al., 2017;Savarino et al., 2013;Ishino et al., 2017b;Savarino et al.,  
15 2007;Alexander et al., 2009). In contrast to Alexander et al. (2009), the model does not significantly underestimate  
16 the  $\Delta^{17}\text{O}(\text{nitrate})$  observations when assuming a bulk ozone isotopic composition ( $\Delta^{17}\text{O}(\text{O}_3)$ ) on the order of 25‰ (see  
17 Figure 2d in Alexander et al. (2009)). The increase in modeled  $\Delta^{17}\text{O}(\text{nitrate})$  is due to increased importance of  $\text{O}_3$  in  
18  $\text{NO}_x$  cycling (85% below 1 km) compared to Alexander et al. (2009) (80% below 1 km altitude), and an increase in  
19 the number and fractional importance of nitrate formation pathways that yield relatively high values of  $\Delta^{17}\text{O}(\text{nitrate})$   
20 (red pathways in Fig. 1). Although  $\text{XO}$  species themselves are only a minor NO oxidation pathway (1%), the addition  
21 of reactive halogen chemistry in the model has altered the relative abundance of  $\text{O}_3$  and  $\text{HO}_x$  (Sherwen et al., 2016) in  
22 such a way as to increase the modeled  $\Delta^{17}\text{O}(\text{NO}_x)$ . The Alexander et al. (2009) study used GEOS-Chem v8-01-01,  
23 which included tropospheric nitrate formation from the  $\text{NO} + \text{OH}$ ,  $\text{N}_2\text{O}_5 + \text{H}_2\text{O}$ , and  $\text{NO}_3 + \text{HC}$  pathways only. An  
24 increased importance of  $\text{N}_2\text{O}_5$  hydrolysis (R4) and additional nitrate formation pathways that yield relatively high  
25 values of  $\Delta^{17}\text{O}(\text{nitrate})$  (R5, R6, R8, and R10) in the present study also explain the increase in modeled  $\Delta^{17}\text{O}(\text{nitrate})$   
26 relative to Alexander et al. (2009). An increase in the average  $A$  value from 0.80 to 0.85 would tend to increase the

1 calculated  $\Delta^{17}\text{O}(\text{nitrate})$  on the order of 2‰ ( $0.05 \times \Delta^{17}\text{O}(\text{O}_3^*)$ ), suggesting that the increase in the relative importance  
2 of the terminal reactions R4, R5, R6, R8, and R10 explains the majority of the difference between the results presented  
3 here compared to (Alexander et al., 2009). Assuming a value of 35‰ for bulk  $\Delta^{17}\text{O}(\text{O}_3)$  in the model that did not  
4 include reactive halogen chemistry or heterogeneous reactions in cloud water produced good agreement between  
5 modeled and observed  $\Delta^{17}\text{O}(\text{nitrate})$  in Alexander et al. (2009); however, in the current version of the model this bulk  
6 isotopic assumption leads to a model overestimate at nearly all locations (Figure S6). The “cloud chemistry” model  
7 shows somewhat better agreement with the observations ( $R^2 = 0.51$  in Figure 5) compared to the “standard” model  
8 ( $R^2 = 0.48$  in Figure S3). Improved agreement with the observations occurs in the mid- to high-latitudes (Figures 6  
9 and S4) is due to addition of  $\text{N}_2\text{O}_5$  hydrolysis in clouds (Figures 3 and S6).

10

11 The mean  $\Delta^{17}\text{O}(\text{nitrate})$  value of the observations ( $27.7 \pm 5.0\text{‰}$ ) shown in Figure 5 is not significantly different from  
12 the modeled values at the location of the observations ( $28.6 \pm 4.5\text{‰}$ ); however, the range of  $\Delta^{17}\text{O}(\text{nitrate})$  values of  
13 the observations (10.9 – 40.6‰) is larger than in the model (19.6 – 37.6‰). As previously noted in Savarino et al.  
14 (2007), the maximum observed  $\Delta^{17}\text{O}(\text{nitrate})$  value (40.6‰) is not possible given our isotope assumption for the  
15 terminal oxygen atom of ozone ( $\Delta^{17}\text{O}(\text{O}_3^*) = 39\text{‰}$ ); however, it is theoretically possible given the approximately 2‰  
16 uncertainty in observed  $\Delta^{17}\text{O}(\text{O}_3^*)$ . A value of  $\Delta^{17}\text{O}(\text{nitrate}) = 41\text{‰}$  is possible if  $\Delta^{17}\text{O}(\text{O}_3^*) = 41\text{‰}$  and all oxygen  
17 atoms of nitrate originate from ozone ( $A = 1$  and all nitrate forms from R2 and/or R5). Although this may be possible  
18 for nitrate formed locally in the Antarctic winter due to little to no sunlight, lack of local  $\text{NO}_x$  sources during Antarctic  
19 winter makes it unlikely that all nitrate observed in Antarctica forms locally. Long-range transport from lower latitudes  
20 and/or the stratosphere likely contributes to nitrate observed in Antarctica during winter (Lee et al., 2014). Observed  
21  $\Delta^{17}\text{O}(\text{nitrate}) > 39\text{‰}$  (in Antarctica) has been suggested to be due to transport of nitrate from the stratosphere (Savarino  
22 et al., 2007), as stratospheric  $\text{O}_3$  is expected to have a higher  $\Delta^{17}\text{O}(\text{O}_3)$  value than ozone produced in the troposphere  
23 (Krankowsky et al., 2000; Mauersberger et al., 2001; Lyons, 2001). Indeed, the model underestimates the observations  
24 at Dumont d’Urville (DDU) and the South Pole (both in Antarctica) during winter and spring (Figure 6), when and  
25 where the stratospheric contribution is expected to be most important (Savarino et al., 2007). The model underestimate  
26 in Antarctica may also be due to model underestimates of  $\text{BrO}$  column (Chen et al., 2017) and ozone abundance  
27 (Sherwen et al., 2016) in the southern high latitudes. The largest model overestimates occur at Mt. Lulin, Taiwan

1 (Figures 5 and 6). Based on nitrogen isotope observations ( $\delta^{15}\text{N}$ ), nitrate at Mt. Lulin is thought to be influenced by  
2 anthropogenic nitrate emitted in polluted areas of mainland China and transported to Mt. Lulin, rather than local nitrate  
3 production (Guha et al., 2017). However, observations of  $\Delta^{17}\text{O}(\text{nitrate})$  in autumn and winter in Beijing suggest much  
4 higher values ( $30.6 \pm 1.8\text{\textperthousand}$ ) than was measured at Mt. Lulin ( $15 - 30\text{\textperthousand}$  in winter). A potential reason for the model  
5 overestimate of the observed values at Mt. Lulin could be qualitatively explained by transport of nitrate formed in the  
6 free troposphere to this high altitude location, where the high  $\Delta^{17}\text{O}(\text{nitrate})$  producing pathways (R4-R8) should be  
7 negligible due to minimal aerosol surface area for heterogeneous chemistry. Low  $\Delta^{17}\text{O}(\text{nitrate})$  values from nitrate  
8 formed at higher altitudes and transported to Mt. Lulin would not be accounted for in the model since the isotopes are  
9 not transported. The model compares better to the mid-latitude locations close to pollution sources (La Jolla and  
10 Princeton), although the model overestimates wintertime  $\Delta^{17}\text{O}(\text{nitrate})$  in Princeton, NJ, USA by up to  $6\text{\textperthousand}$  and  
11 underestimates winter time  $\Delta^{17}\text{O}(\text{nitrate})$  in La Jolla, CA, USA by up to  $4\text{\textperthousand}$ . The model overestimate at Princeton  
12 during winter could be due to the fact that these are precipitation samples and not ambient aerosol samples, and thus  
13 may reflect nitrate formed at altitudes higher than we are sampling in the model. The underestimate at La Jolla, CA  
14 could be due to underestimates in reactive chlorine chemistry in the model, which would tend to increase  $\Delta^{17}\text{O}(\text{nitrate})$   
15 by increasing nitrate formation by the hydrolysis of halogen nitrates (R6) in this coastal location. The model  
16 underestimates the  $\Delta^{17}\text{O}(\text{nitrate})$  observations at Cape Verde in late summer/early autumn by up to  $6\text{\textperthousand}$  (Savarino et  
17 al., 2013). Comparison with results from the steady-state model employed in Savarino et al. (2013) suggests that the  
18 low bias could be due to an underestimate of nitrate formation via  $\text{NO}_3 + \text{DMS}$  (R2). The steady-state model in  
19 Savarino et al. (2013) agreed with observations when R2 represented about one-third of total nitrate formation. The  
20 model results presented here have R2 representing about 15% of total nitrate formation in this season. An  
21 underestimate of the relative importance of R2 could result from a model underestimate of atmospheric DMS  
22 abundances.

23

#### 24 **4. Model uncertainties**

25 The uncertainty in the two most important nitrate formation pathways,  $\text{NO}_2 + \text{OH}$  and  $\text{N}_2\text{O}_5$  hydrolysis, and their  
26 impacts on  $\text{NO}_x$  and oxidant budgets, have been examined and discussed elsewhere (Macintyre and Evans,  
27 2010; Newsome and Evans, 2017; Holmes et al., 2019). The impacts of the formation and hydrolysis of halogen nitrates

1 on global NO<sub>x</sub> and oxidant budgets have also been previously examined (Sherwen et al., 2016). Here we focus on  
2 three additional processes using a set of model sensitivity studies. First, we examine the importance of the third most  
3 important nitrate production pathway on the global scale as predicted by the “standard” model, NO<sub>2</sub> aerosol uptake  
4 and hydrolysis, and its implications for the global NO<sub>x</sub>, nitrate, and oxidant budgets. Second, we examine the role of  
5 changing anthropogenic NO<sub>x</sub> emissions over a 15-year period (2000 to 2015) on the relative importance of the  
6 formation of inorganic nitrate from the hydrolysis of organic nitrates. Finally, we examine the role of aerosol nitrate  
7 photolysis on the relative importance of different nitrate formation pathways. The impact of aerosol nitrate photolysis  
8 on NO<sub>x</sub> and oxidant budgets has been examined in detail elsewhere (Kasibhatla et al., 2018).

9

#### 10 **4.1 Heterogeneous uptake and hydrolysis of NO<sub>2</sub>**

11 Heterogeneous uptake of NO<sub>2</sub> to form HNO<sub>3</sub> and HONO is the third most important nitrate formation pathway in the  
12 “standard” model on the global scale (Figure 1). The reaction probability ( $\gamma_{NO_2}$ ) measured in laboratory studies ranges  
13 between  $10^{-8}$  to  $10^{-4}$  depending on aerosol chemical composition (Lee and Tang, 1988; Crowley et al., 2010; Gutzwiler  
14 et al., 2002; Yabushita et al., 2009; Abbatt and Waschewsky, 1998; Burkhardt et al., 2015; Broske et al., 2003; Li et al.,  
15 2018a; Xu et al., 2018). A value of  $\gamma_{NO_2} = 10^{-4}$  is used in the “standard” model, which is at the high end of the reported  
16 range. A molar yield of 0.5 for both HNO<sub>3</sub> and HONO formation is assumed in the model based on laboratory studies  
17 and hypothesized reaction mechanisms (Finlayson-Pitts et al., 2003; Jenkin et al., 1988; Ramazan et al., 2004; Yabushita  
18 et al., 2009). However, both the reaction rate and mechanism of this reaction and its dependence on chemical  
19 composition and pH is still not well understood (Spataro and Ianniello, 2014).

20

21 The “cloud chemistry” simulation uses a reaction probability formulation for aerosol uptake of NO<sub>2</sub> ( $\gamma_{NO_2}$ ) that  
22 depends on aerosol chemical composition, ranging from  $\gamma_{NO_2} = 10^{-8}$  for dust to  $\gamma_{NO_2} = 10^{-4}$  for black carbon based on  
23 recent laboratory studies (Holmes et al., 2019). The updated NO<sub>2</sub> reaction probability results in a negligible (<1%)  
24 importance of this reaction for nitrate formation, compared to 12% contribution in the “standard” model. The “cloud  
25 chemistry” simulation significantly increases the fractional importance of N<sub>2</sub>O<sub>5</sub> hydrolysis (from 28 to 41%, globally  
26 below 1 km altitude) compared to the “standard” simulation, in part due to decreased competition from NO<sub>2</sub> hydrolysis  
27 and in part due to increased N<sub>2</sub>O<sub>5</sub> hydrolysis in clouds. To evaluate the relative importance of competition from NO<sub>2</sub>  
28 hydrolysis and the addition of N<sub>2</sub>O<sub>5</sub> hydrolysis in clouds, we perform a model sensitivity study that is the same as the

1 “standard” simulation but decreases the reaction probability of  $\text{NO}_2$  hydrolysis on aerosol ( $\gamma_{\text{NO}_2} = 10^{-7}$ ), without adding  
2  $\text{N}_2\text{O}_5$  hydrolysis in clouds. Similar to the “cloud chemistry” simulation, using  $\gamma_{\text{NO}_2} = 10^{-7}$  renders  $\text{NO}_2$  hydrolysis a  
3 negligible nitrate formation pathway, and increases the relative importance of  $\text{N}_2\text{O}_5$  hydrolysis from 28% to 37%.  
4 This suggests that reduced competition from  $\text{NO}_2$  hydrolysis is the main reason for the increased importance of  $\text{N}_2\text{O}_5$   
5 hydrolysis in the “cloud chemistry” simulation, though the addition of heterogeneous reactions on clouds also plays a  
6 role.

7

8  $\text{NO}_2$  hydrolysis represents a significant source of HONO in the “standard” model simulation; the reduced  $\text{NO}_2$  reaction  
9 probability from  $\gamma_{\text{NO}_2} = 10^{-4}$  to  $\gamma_{\text{NO}_2} = 10^{-7}$  results in a reduction of HONO below 1 km altitude by up to 100% over  
10 the continents, with relatively small (up to 1 ppb) changes in nitrate concentrations (Figure 7). The reduction in the  
11 rate of heterogeneous  $\text{NO}_2$  uptake leads to reductions in OH where this reaction was most important in the model  
12 (over China and Europe) due to reductions in HONO, but leads to increases in OH elsewhere due to increases in ozone  
13 (by up to a few ppb) resulting from small increases in the  $\text{NO}_x$  lifetime due to a reduction in the  $\text{NO}_x$  sink (Figure 8).  
14 Similar changes in HONO are seen when comparing the “standard” and “cloud chemistry” simulation (not shown).  
15 Increased importance of  $\text{N}_2\text{O}_5$  hydrolysis in both the “cloud chemistry” simulation and the simulation without cloud  
16 chemistry but with a reduced reaction probability for  $\text{NO}_2$  hydrolysis increases modeled annual-mean  $\Delta^{17}\text{O}(\text{nitrate})$   
17 by up to 3‰ in China where this reaction is most important. This improves model agreement with monthly-mean  
18 observations of  $\Delta^{17}\text{O}(\text{nitrate})$  in Beijing (He et al., 2018a) (Figures 5 and S3).

19

20 The product yields of  $\text{NO}_2$  hydrolysis are also uncertain. Jenkin et al. (1988) proposed the formation of a water  
21 complex,  $\text{NO}_2 \cdot \text{H}_2\text{O}$ , leading to the production of HONO and  $\text{HNO}_3$ . Finlayson-Pitts et al. (2003) and Ramazan et al.  
22 (2004) proposed the formation of the dimer  $\text{N}_2\text{O}_4$  on the surface, followed by isomerization to form  $\text{NO}^+\text{NO}_3^-$ .  
23 Reaction of  $\text{NO}^+\text{NO}_3^-$  with  $\text{H}_2\text{O}$  results in the formation of HONO and  $\text{HNO}_3$ . Laboratory experiments by Yabushita  
24 et al. (2009) suggested that dissolved anions catalyzed the dissolution of  $\text{NO}_2$  to form a radical intermediate  $\text{X-NO}_2^-$   
25 (where  $\text{X} = \text{Cl, Br, or I}$ ) at the surface followed by reaction with  $\text{NO}_2(\text{g})$  to form HONO and  $\text{NO}_3^-$ . These experiments  
26 described above were performed at  $\text{NO}_2$  concentrations much higher than exist in the atmosphere (10 – 100 ppm)  
27 (Yabushita et al., 2009;Finlayson-Pitts et al., 2003;Ramazan et al., 2004). A laboratory study utilizing isotopically  
28 labeled water to investigate the reaction mechanism suggested that the formation of HONO resulted from the reaction

1 between adsorbed  $\text{NO}_2$  and  $\text{H}^+$ , while the formation of  $\text{HNO}_3$  resulted from the reaction between adsorbed  $\text{NO}_2$  and  
2  $\text{OH}^-$ , and did not involve the  $\text{N}_2\text{O}_4$  intermediate (Gustafsson et al., 2009). Results from Gustafsson et al. (2009)  
3 suggest an acidity-dependent yield of  $\text{HONO}$  and  $\text{HNO}_3$ , favoring  $\text{HONO}$  at low pH values. A recent study in the  
4 northeast U.S. during winter found that modeled nitrate abundance was overestimated using a molar yield of 0.5 for  
5  $\text{HONO}$  and  $\text{HNO}_3$ , and the model better matched the observations of  $\text{NO}_2$  and nitrate when assuming a molar yield of  
6 1.0 for  $\text{HONO}$  (Jaeglé et al., 2018). Particles were acidic ( $\text{pH} < 2$ ) during this measurement campaign (Guo et al.,  
7 2017;Shah et al., 2018), which may favor  $\text{HONO}$  production over  $\text{HNO}_3$ .

8  
9 We examine the potential importance of this acidity-dependent yield by implementing a pH-dependent product yield  
10 in two separate sensitivity simulations, first using an  $\text{NO}_2$  aerosol uptake reaction probability of  $\gamma = 10^{-4}$  as in the  
11 “standard” simulation and second with  $\gamma_{\text{NO}_2} = 10^{-7}$ . The acidity-dependent yield for  $\text{HONO}$  and  $\text{HNO}_3$  formation is  
12 based on the laboratory study by Gustafsson et al. (2009). We use aerosol pH calculated from ISORROPIA II  
13 (Fountoukis and Nenes, 2007) to calculate the concentration of  $[\text{H}^+]$  and  $[\text{OH}^-]$  in aerosol water. The yield of  $\text{HONO}$   
14 ( $\gamma_{\text{HONO}}$ ) from heterogeneous uptake of  $\text{NO}_2$  on aerosol surfaces is calculated according to E3:

$$15 \quad \gamma_{\text{HONO}} = \frac{[\text{H}^+]}{[\text{H}^+] + [\text{OH}^-]} \quad (\text{E3})$$

16 where  $[\text{H}^+]$  and  $[\text{OH}^-]$  are in units of M. The yield of  $\text{HNO}_3$  from this reaction is equal to  $(1 - \gamma_{\text{HONO}})$ . E3 yields values  
17 of  $\gamma_{\text{HONO}}$  near unity for aerosol pH values less than 6, decreasing rapidly to zero between pH values between 6-8  
18 (Figure S8). Calculated aerosol pH values are typically  $< 6$  in the model except in remote regions far from  $\text{NO}_x$   
19 sources (Figure S9), favoring the product  $\text{HONO}$ .

20  
21 The acidity-dependent yield implemented in the “standard” simulation with  $\gamma_{\text{NO}_2} = 10^{-4}$  increases  $\text{HONO}$   
22 concentrations by up to 1 ppbv in China where this reaction is most important (Figure 9). Fractional increases in  
23  $\text{HONO}$  exceed 100% in remote locations (Figure 9). Increased  $\text{HONO}$  leads to increases in  $\text{OH}$  on the order of 10 –  
24 20% in most locations below 1 km altitude, while ozone concentrations increase in most locations by up to several  
25 ppbv (Figure 9). The exception is the southern high latitudes; likely due to decreased formation and thus transport of  
26 nitrate to remote locations. The impact on  $\text{NO}_x$  and nitrate budgets is relatively minor. The global, annual mean  $\text{NO}_x$   
27 burden near the surface (below 1 km) increases slightly (+2%) as a result of the decreased rate of conversion of  $\text{NO}_2$   
28 to nitrate; the change to the global tropospheric burden is negligible. Annual-mean surface nitrate concentrations

1 show small decreases up to 1 ppbv in China where this reaction is most important in the model; impacts on nitrate  
2 concentrations over a shorter time period may be more significant (Jaeglé et al., 2018). The fraction of  $\text{HNO}_3$  formed  
3 from  $\text{NO}_2 + \text{OH}$  (49%) increases due to increases in OH from the HONO source. The fraction of  $\text{HNO}_3$  formation  
4 from the uptake and hydrolysis of  $\text{N}_2\text{O}_5$  also increases (from 28% to 32%) due to reductions in the nighttime source  
5 of nitrate from  $\text{NO}_2$  hydrolysis. The calculated mean  $\Delta^{17}\text{O}(\text{nitrate})$  at the location of the observations shown in Figure  
6 5 ( $27.9 \pm 5.0\text{\textperthousand}$ ) is not significantly impacted due to compensating effects from changes in both high- and low-  
7 producing  $\Delta^{17}\text{O}(\text{nitrate})$  values. Modeled monthly mean  $\Delta^{17}\text{O}(\text{nitrate})$  in China, where  $\text{NO}_2$  hydrolysis is most  
8 important decreases by 0.9-1.9%, and is biased low by 1.8-3.4%.

9  
10 Using a combination of both the low reaction probability ( $\gamma = 10^{-7}$ ) and the acidity-dependent yield gives similar results  
11 as using  $\gamma = 10^{-7}$  and assuming a molar yield of 0.5 for HONO and  $\text{HNO}_3$  (not shown). In other words, including a  
12 pH-dependent product yield rather than a yield of 0.5 for HONO and nitrate results in negligible differences for  
13 oxidants,  $\text{NO}_x$  and nitrate abundances when the reaction probability ( $\gamma_{\text{NO}_2}$ ) is low.

14  
15 **4.2 Hydrolysis of organic nitrates ( $\text{RONO}_2$ )**  
16 Anthropogenic  $\text{NO}_x$  emissions have been increasing in China and decreasing in the U.S. and Europe (Richter et al.,  
17 2005; Hoesly et al., 2018b), with implications for the relative importance of inorganic and organic nitrate formation as  
18 a sink for  $\text{NO}_x$  (Zare et al., 2018). To examine the impacts of recent changes in anthropogenic  $\text{NO}_x$  emissions for  
19 nitrate formation pathways, we run the “standard” model using the year 2000 emissions and meteorology after a 1-  
20 year model spin up, and compare the results to the “standard” model simulation run in the year 2015. This time-period  
21 encompasses significant changes in anthropogenic  $\text{NO}_x$  emissions in the U.S., Europe, and China, and encompasses  
22 most of the time period of the observations shown in Figures 5 and 6. Total, global anthropogenic emissions of  $\text{NO}_x$   
23 are slightly lower in the 2000-year simulation ( $30 \text{ Tg N yr}^{-1}$ ) compared to the year 2015 simulation ( $31 \text{ Tg N yr}^{-1}$ ) due  
24 to decreases in North America and Europe, counteracted by increases in Asia (Figure S10). This leads to increases of  
25 less than 10% in the annual-mean, fractional importance of the source of nitrate from the hydrolysis of organic nitrates  
26 in the U.S., and corresponding decreases of less than 10% over China (Figure 10). Relatively small changes (< 10%)  
27 in nitrate formation pathways yield small changes (< 2%) in modeled annual-mean  $\Delta^{17}\text{O}(\text{nitrate})$  between the year  
28 2000 and 2015, differences in  $\Delta^{17}\text{O}(\text{nitrate})$  over shorter time periods may be larger. Changes in the formation of

1 nitrate from the hydrolysis of  $\text{RONO}_2$  remains unchanged globally, as increases in the U.S. and Europe and decreases  
2 in China counteract one another.

3

4 **4.3 Photolysis of aerosol nitrate**

5 Observations have demonstrated that aerosol nitrate can be photolyzed at rates much faster than  $\text{HNO}_3(\text{g})$  (Reed et al.,  
6 2017;Ye et al., 2016); however, the magnitude of the photolytic rate constant is uncertain. We examine the  
7 implications of this process for global nitrate formation pathways by implementing the photolysis of aerosol nitrate as  
8 described in Kasibhatla et al. (2018) into the “standard” model simulation, scaling the photolytic rate constant for both  
9 fine- and coarse-mode aerosol nitrate to a factor of 25 times higher than that for  $\text{HNO}_3(\text{g})$  (Kasibhatla et al.,  
10 2018;Romer et al., 2018), with a molar yield of 0.67 for  $\text{HONO}$  and 0.33 for  $\text{NO}_x$  production. The global, annual  
11 mean  $\text{NO}_x$  burden near the surface (below 1 km) increases slightly (+2%) as a result of the photolytic recycling of  
12 nitrate to  $\text{NO}_x$ , similar to Kasibhatla et al. (2018). Aerosol nitrate photolysis results in only small impacts on the  
13 relative importance of nitrate formation pathways (< 2%) likely due to simultaneous increases in  $\text{O}_3$  and  $\text{OH}$   
14 (Kasibhatla et al., 2018), which in turn yields small impacts on calculated  $\Delta^{17}\text{O}(\text{nitrate})$  at the location of the  
15 observations shown in Figure 5 ( $27.9 \pm 5.0\text{\textperthousand}$ ). Nitrate photolysis itself has minimal impact on  $\Delta^{17}\text{O}(\text{nitrate})$  because  
16 it is a mass-dependent process (McCabe et al., 2005).

17

18 **5 Conclusions**

19 Observations of  $\Delta^{17}\text{O}(\text{nitrate})$  can be used to help quantify the relative importance of different nitrate formation  
20 pathways. Interpretation of  $\Delta^{17}\text{O}(\text{nitrate})$  requires knowledge of  $\Delta^{17}\text{O}(\text{O}_3)$ . Previous modeling studies showed good  
21 agreement between observed and modeled  $\Delta^{17}\text{O}(\text{nitrate})$  when assuming a bulk oxygen isotopic composition of ozone  
22 ( $\Delta^{17}\text{O}(\text{O}_3)$ ) of  $35\text{\textperthousand}$  based on laboratory and modeling studies (Morton et al., 1990;Thiemens, 1990;Lyons, 2001).  
23 However, recent and spatially widespread observations of  $\Delta^{17}\text{O}(\text{O}_3)$  have consistently shown  $\Delta^{17}\text{O}(\text{O}_3) = 26 \pm 1\text{\textperthousand}$ ,  
24 suggesting that models are underestimating the role of ozone relative to  $\text{HO}_x$  in  $\text{NO}_x$  chemistry. We utilize a global  
25 compilation of observations of  $\Delta^{17}\text{O}(\text{nitrate})$  to assess the representation of nitrate formation in a global chemical  
26 transport model (GEOS-Chem), assuming that the bulk oxygen isotopic composition of ozone ( $\Delta^{17}\text{O}(\text{O}_3)$ ) =  $26\text{\textperthousand}$ .  
27 The modeled  $\Delta^{17}\text{O}(\text{nitrate})$  is roughly consistent with observations, with a mean modeled and observed  $\Delta^{17}\text{O}(\text{nitrate})$   
28 of  $(28.6 \pm 4.5\text{\textperthousand})$  and  $(27.6 \pm 5.0\text{\textperthousand})$ , respectively, at the locations of the observations. Improved agreement between

1 modeled and observed  $\Delta^{17}\text{O}(\text{nitrate})$  is due to increased importance of ozone versus  $\text{HO}_2$  and  $\text{RO}_2$  in  $\text{NO}_x$  cycling and  
2 an increase in the number and importance of nitrate production pathways that yield high  $\Delta^{17}\text{O}(\text{nitrate})$  values. The  
3 former may be due to implementation of tropospheric reactive halogen chemistry in the model, which impacts ozone  
4 and  $\text{HO}_x$  abundances. The latter is due mainly to increases in the relative importance of  $\text{N}_2\text{O}_5$  hydrolysis, with the  
5 hydrolysis of halogen nitrates also playing an important role in remote regions.

6

7 The main nitrate formation pathways in the model below 1 km altitude are from  $\text{NO}_2 + \text{OH}$  and  $\text{N}_2\text{O}_5$  hydrolysis (both  
8 41%). The relative importance of global nitrate formation from the hydrolysis of halogen nitrates and hydrogen-  
9 abstraction reactions involving the nitrate radical ( $\text{NO}_3$ ) are of similar magnitude (~5%). The formation of nitrate  
10 from the hydrolysis of organic nitrate has increased slightly in the U.S. and decreased in China (changes <10%) due  
11 to changing  $\text{NO}_x$  emissions from the year 2000 to 2015, although the global mean fractional importance (6%) remains  
12 unchanged as the regional changes counteract one another. Nitrate formation via heterogeneous  $\text{NO}_2$  and  $\text{NO}_3$  uptake  
13 and  $\text{NO}_2 + \text{HO}_2$  are negligible (<2%). Although aerosol nitrate photolysis has important implications for  $\text{O}_3$  and  $\text{OH}$ ,  
14 the impacts on nitrate formation pathways are small.

15

16 The model parameterization for heterogeneous uptake of  $\text{NO}_2$  has significant impacts on  $\text{HONO}$  and oxidants ( $\text{OH}$   
17 and ozone) in the model.  $\text{HONO}$  production from this reaction has been suggested to be an important source of  $\text{OH}$   
18 in Chinese haze due to high  $\text{NO}_x$  and aerosol abundances (Hendrick et al., 2014; Tong et al., 2016; Wang et al., 2017),  
19 with implications for the gas-phase formation of sulfate aerosol from the oxidation of sulfur dioxide by  $\text{OH}$  (Shao et  
20 al., 2019; Li et al., 2018b). More recent laboratory studies suggest that the reaction probability of  $\text{NO}_2$  on aerosols is  
21 lower than that previously used in the model. Using an  $\text{NO}_2$  reaction probability formulation that depends on the  
22 chemical composition of aerosols as described in Holmes et al. (2019) renders this reaction negligible for nitrate  
23 formation, and has significant implications for modeled  $\text{HONO}$ , ozone, and  $\text{OH}$ . Although uncertainty also exists in  
24 the relative yield of nitrate and  $\text{HONO}$  from this reaction, the impacts of this assumption are negligible when we use  
25 these updated  $\text{NO}_2$  reaction probabilities. Observations of  $\Delta^{17}\text{O}(\text{nitrate})$  in Chinese haze events during winter (He et  
26 al., 2018b) may help to quantify the importance of this nitrate production pathway in a region where the model predicts  
27 it is significant.

28

1 Data availability: The GEOS-Chem model is available at <http://acmg.seas.harvard.edu/geos>.  
2  
3 Author contributions: B.A. designed the study and performed the model simulations and calculations. All other  
4 authors provided model code and contributed to writing and analysis.  
5

6 Competing interests: The authors declare that they have no conflict of interest.  
7

8 **Acknowledgements:**

9 B.A. acknowledges NSF AGS 1644998 and 1702266 and helpful discussions with Joël Savarino and Ron Cohen.  
10 C.D.H. acknowledges the NASA New Investigator Program grant NNX16AI57G. J.A.F. acknowledges Australian  
11 Research Council funding DP160101598.  
12

13 **References**

14 Abbatt, J. P. D., and Waschewsky, G. C. G.: Heterogeneous interactions of OHBr, HNO<sub>3</sub>, O<sub>3</sub>, and NO<sub>2</sub> with  
15 deliquescent NaCl aerosols at room temperature, *J. Phys. Chem. A*, 102, 3719-3725, 1998.  
16 Alexander, B., Savarino, J., Kreutz, K. J., and Thiemens, M. H.: Impact of preindustrial biomass-burning  
17 emissions on the oxidation pathways of tropospheric sulfur and nitrogen, *J. Geophys. Res.*, 109, D08303,  
18 doi: 10.1029/2003JD004218, 2004.  
19 Alexander, B., Hastings, M. G., Allman, D. J., Dachs, J., Thornton, J. A., and Kunasek, S. A.: Quantifying  
20 atmospheric nitrate formation pathways based on a global model of the oxygen isotopic composition  
21 ( $\Delta^{17}\text{O}$ ) of atmospheric nitrate, *Atmos. Chem. Phys.*, 9, 5043-5056, 10.5194/acp-9-5043-2009, 2009.  
22 Atkinson, R.: Atmospheric chemistry of VOCs and NO<sub>x</sub>, *Atm. Env.*, 34, 2063-2101, 10.1016/S1352-  
23 2310(99)00460-4, 2000.  
24 Berhanu, T. A., Savarino, J., Bhattacharya, S. K., and Vicars, W. C.:  $^{17}\text{O}$  excess transfer during the NO<sub>2</sub> + O<sub>3</sub>  
25 --> NO<sub>3</sub> + O<sub>2</sub> reaction, *J. Chem. Phys.*, 136, 044311, doi: 10.1063/1.3666852, 2012.  
26 Bertram, T. H., and Thornton, J. A.: Toward a general parameterization of N<sub>2</sub>O<sub>5</sub> reactivity on aqueous  
27 particles: the competing effects of particle liquid water, nitrate and chloride, *Atmos. Chem. Phys.*, 9,  
28 8351-8363, 10.5194/acp-9-8351-2009, 2009.  
29 Bey, I., Jacob, D. J., Yantosca, R. M., Logan, J. A., Field, B. D., Fiore, A. M., Li, Q., Liu, H. Y., Mickley, L. J.,  
30 and Schultz, M. G.: Global modeling of tropospheric chemistry with assimilated meteorology: Model  
31 description and evaluation, *J. Geophys. Res.*, 106, 23073-23095, 2001.  
32 Bhattacharya, S. K., Pandey, A., and Savarino, J.: Determination of intramolecular isotope distribution of  
33 ozone by oxidation reaction with silver metal, *J. Geophys. Res.*, 113, D03303, doi:10.1029/2006JF008309,  
34 2008.  
35 Bhattacharya, S. K., Savarino, J., Michalski, G., and Liang, M.-C.: A new feature in the internal heavy  
36 isotope distribution in ozone, *J. Chem. Phys.*, 141, 10.1063/1.4895614, 2014.  
37 Brenninkmeijer, C. A. M., Janssen, C., Kaiser, J., Rockmann, T., Rhee, T. S., and Assonov, S. S.: Isotope  
38 effects in the chemistry of atmospheric trace compounds, *Chemical Reviews*, 102, 5125-5161, 2003.

1 Broske, R., Kleffmann, J., and Wiesen, P.: Heterogeneous conversion of NO<sub>2</sub> on secondary organic  
2 aerosol surfaces: A possible source of nitrous acid (HONO) in the atmosphere?, *Atmos. Chem. Phys.*, 3,  
3 469-474, 10.5194/acp-3-469-2003, 2003.

4 Brothers, L. A., Dominguez, G., Fabian, P., and Thiemens, M. H.: Using multi-isotope tracer methods to  
5 understand the sources of nitrate in aerosols, fog and river water in Podocarpus National Forest,  
6 Ecuador, *Eos Trans. AGU*, 89, Abstract A11C-0136, 2008.

7 Browne, E. C., and Cohen, R. C.: Effects of biogenic nitrate chemistry on the NO<sub>x</sub> lifetime in remost  
8 continental regions, *Atmos. Chem. Phys.*, 12, 11917-11932, 10.5194/acp-12-11917-2012, 2014.

9 Burkhardt, J. F., Sander, S. P., Abbatt, J. P. D., Barker, J. R., Huie, R. E., Kolb, C. E., Kurylo, M. J., Orkin, V. L.,  
10 Wilmouth, D. M., and Wine, P. H.: Chemical Kinetics and Photochemical Data for Use in Atmospheric  
11 Studies, Jet Propulsion Laboratory, Pasadena, CA, USA, 2015.

12 Burkholder, J. B., Sander, S. P., Abbatt, J. P. D., Barker, J. R., Huie, R. E., Kolb, C. E., Kurylo, M. J., Orkin, V.  
13 L., Wilmouth, D. M., and Wine, P. H.: Chemical kinetics and photochemical data for use in atmospheric  
14 studies: evaluation number 18, Jet Propulsion Laboratory, Pasadena, CA, 2015.

15 Butkovskaya, N. I., Kukui, A., Pouvesle, N., and Le Bras, G.: Formation of Nitric Acid in the Gas-Phase HO<sub>2</sub>  
16 + NO Reaction: Effects of Temperature and Water Vapor, *J. Phys. Chem. A*, 109, 6509-6520,  
17 10.1021/jp051534v, 2005.

18 Chen, Q., Schmidt, J. A., Shah, V., Jaeglé, L., Sherwen, T., and Alexander, B.: Sulfate production by  
19 reactive bromine: Implications for the global sulfur and reactive bromine budgets, *Geophys. Res. Lett.*,  
20 44, 7069-7078, 10.1002/2017GL073812, 2017.

21 Chen, Q., Edebeli, J., McNamara, S. M., Kulju, K., May, N. W., Bertman, S. P., Thanekar, S., Fuentes, J. D.,  
22 and Pratt, K. A.: HONO, Particulate Nitrite, and Snow Nitrite at a Midlatitude Urban Site during  
23 Wintertime, *ACS Earth Space Chem.*, 10.1021/acsearthspacechem.9b00023, 2019.

24 Connell, P., and Johnston, H. S.: Thermal dissociation of N<sub>2</sub>O<sub>5</sub> in N<sub>2</sub>, *Geophys. Res. Lett.*, 6, 553-556,  
25 1979.

26 Costa, A. W., Michalski, G., Schauer, A. J., Alexander, B., Steig, E. J., and Shepson, P. B.: Analysis of  
27 atmospheric inputs of nitrate to a temperate forest ecosystem from  $\Delta^{17}\text{O}$  isotope ratio measurements,  
28 *Geophys. Res. Lett.*, 38, L15805, doi:10.1029/2011GL047539, 2011.

29 Crowley, J. N., Ammann, M., Cox, R. A., Hynes, R. G., Jenkin, M. E., Mellouki, A., Rossi, M. J., Troe, J., and  
30 Wallington, T. J.: Evaluated kinetic and photochemical data for atmospheric chemistry: Volume V –  
31 heterogeneous reactions on solid substrates, *Atmos. Chem. Phys.*, 10, 9059-9223, 10.5194/acp-10-9059-  
32 2010, 2010.

33 Domine, F., and Shepson, P. B.: Air-Snow Interactions and Atmospheric Chemistry, *Science*, 297, 1506,  
34 2002.

35 Dubey, M. K., Mohrschladt, R., Donahue, N. M., and Anderson, J. G.: Isotope-specific kinetics of hydroxyl  
36 radical (OH) with water (H<sub>2</sub>O): Testing models of reactivity and atmospheric fractionation, *J. Phys. Chem.*  
37 A, 101, 1494-1500, 1997.

38 Evans, M. J., and Jacob, D. J.: Impact of new laboratory studies of N<sub>2</sub>O<sub>5</sub> hydrolysis on global model  
39 budgets of tropospheric nitrogen oxides, ozone, and OH, *Geophys. Res. Lett.*, 32, L09813,  
40 doi:10.1029/2005GL022469, 2005.

41 Ewing, S. A., Michalski, G., Thiemens, M., Quinn, R. C., Macalady, J. L., Kohl, S., Wankel, S. D., Kendall, C.,  
42 McKay, C. P., and Amundson, R.: Rainfall limit of the N cycle on Earth, *Global Biogeochemical Cycles*, 21,  
43 GB3009, 10.1029/2006gb002838, 2007.

44 Fibiger, D. L., Hastings, M. G., Dibb, J. E., and Huey, L. G.: The preservations of atmospheric nitrate in  
45 snow at Summit, Greenland, *Geophys. Res. Lett.*, 40, 3484-3489, 10.1002/grl.50659, 2013.

46 Finlayson-Pitts, B. J., Wingen, L. M., Sumner, A. L., Syomin, D., and Ramazan, K. A.: The heterogeneous  
47 hydrolysis of NO<sub>2</sub> in laboratory systems and in outdoor and indoor atmospheres: An integrated  
48 mechanism, *Phys. Chem. Chem. Phys.*, 5, 223-242, 2003.

1 Fisher, J. A., Jacob, D. J., Travis, K. R., Kim, P. S., Marais, E. A., Miller, C. C., Yu, K., Zhu, L., Yantosca, R. M.,  
2 Sulprizio, M. P., Mao, J., Wennberg, P. O., Crounse, J. D., Teng, A. P., Nguyen, T. B., St. Clair, J. M., Cohen,  
3 R. C., Romer, P., Nault, B. A., Wooldridge, P. J., Jimenez, J. L., Campuzano-Jost, P., D.A., D., Hu, W.,  
4 Shepson, P. B., Wiong, F., Blake, D. R., Goldstein, A. H., Misztal, P. K., Hanisco, T. F., Wolfe, G. M.,  
5 Ryerson, T. B., Wisthaler, A., and Mikoviny, T.: Organic nitrate chemistry and its implications for  
6 niteogen budgets in an isoprene- and mooterpene-rich atmosphere: constraints from aircraft (SEAC<sup>4</sup>RS)  
7 and ground-based (SOAS) observations in the Southeast US, *Atmos. Chem. Phys.*, 16, 5969-5991,  
8 10.5194/acp-16-5969-2016, 2016.

9 Fisher, J. A., Atlas, E. L., Barletta, B., Meinardi, S., Blake, D. R., Thompson, C. R., Ryerson, T. B., Peischl, J.,  
10 Tzompa-Sosa, Z. A., and Murray, L. T.: Methyl, Ethyl, and Propyl Nitrates: Global Distribution and Impacts  
11 on Reactive Nitrogen in Remote Marine Environments, *J. Geophys. Res.*, 123, 12,429-412,451,  
12 doi.org/10.1029/2018JD029046, 2018.

13 Fountoukis, C., and Nenes, A.: ISORROPIA II: a computationally efficient thermodynamic equilibrium  
14 model for  $K^+$ - $Ca^{2+}$ - $Mg^{2+}$ - $NH_4^+$ - $Na^+$ - $SO_4^{2-}$ - $NO_3^-$ - $Cl^-$ - $H_2O$  aerosols, *Atmos. Chem. Phys.*, 7, 4639-4659, 2007.

15 Geng, L., Cole-Dai, J., Alexander, B., Savarino, J., Schauer, A. J., Steig, E. J., Lin, P., and Zatko, M. C.: On  
16 the origin of the occasional springtime nitrate concentration maximum in Greenland snow, *Atmos.*  
17 *Chem. Phys. Discuss.*, 14, 9401-9437, 10.5194/acpd-14-9401-2014, 2014.

18 Geng, L., Murray, L. T., Mickley, L. J., Lin, P., Fu, Q., Schauer, A. J., and Alexander, B.: Isotopic evidence of  
19 multiple controls on atmospheric oxidants over climate transitions, *Nature*, 546, 133-136,  
20 10.1038/nature22340, 2017.

21 Guha, T., Lin, C. T., Bhattacharya, S. K., Mahajan, A. S., Ou-Yang, C.-F., Lan, Y.-P., Hsu, S. C., and Liang, M.-  
22 C.: Isotopic ratios of nitrate in aerosol samples from Mt. Lulin, a high-altitude station in Central Taiwan,  
23 *Atmos. Env.*, 154, 53-69, 10.1016/j.atmosenv.2017.01.036, 2017.

24 Guo, H., Weber, R. J., and Nenes, A.: High levels of ammonia do not raise fine particle pH sufficiently to  
25 yield nitrogen oxide-dominated sulfate production, *Scientific Reports*, 7, 1-7, 10.1038/s41598-017-  
26 11704-0, 2017.

27 Gustafsson, R. J., Kyakou, G., and Lambert, R. M.: The molecular mechanism of tropospheric nitrous acid  
28 production on mineral dust surfaces, *Chem. Phys. Chem.*, 9, 1390-1393, 10.1002/cphc.200800259, 2009.

29 Gutzwiller, L., George, C., Rossler, E., and Ammann, J.: Reaction Kinetics of  $NO_2$  with Resorcinol and 2,7-  
30 Naphthalenediol in the Aqueous Phase at Different pH, *J. Phys. Chem. A*, 106, 12045-12050,  
31 10.1021/jp026240d, 2002.

32 Hastings, M. G., Sigman, D. M., and Lipschultz, F.: Isotopic evidence for source changes of nitrate in rain  
33 at Bermuda, *J. Geophys. Res.*, 108, 4790, doi:10.1029/2003JD003789, 2003.

34 He, P., Alexander, B., Geng, L., Chi, X., Fan, S., Zhan, H., Kang, H., Zheng, G., Cheng, Y., Su, H., Liu, C., and  
35 Xie, Z.: Isotopic constraints on heterogeneous sulfate production in Beijing haze, *Atmos. Chem. Phys.*, 18,  
36 5515-5528, 10.5194/acp-18-5515-2018 2018a.

37 He, P., Xie, Z., Chi, X., Yu, X., Fan, S., Kang, H., Liu, C., and Zhan, H.: Atmospheric  $\Delta^{17}O(NO_3^-)$  reveals  
38 nocturnal chemistry dominates nitrate production in Beijing haze, *Atmos. Chem. Phys.*, 18, 14465-14476,  
39 10.5194/acp-18-14465-2018, 2018b.

40 Heidenreich, J. E., and Thiemens, M. H.: A non-mass dependent oxygen isotope effect in the production  
41 of ozone from molecular oxygen: The role of molecular symmetry in isotope chemistry, *J. Chem. Phys.*,  
42 84, 2129-2136, 1986.

43 Hendrick, F., Muller, J.-F., Clemer, K., Wang, P., De Maziere, M., Fayt, C., Gielen, C., Hermans, C., Ma, J.  
44 Z., Pinardi, G., Stavrakou, T., Vlemmix, T., and Van Roosendaal, M.: Four years of ground-based MAX-  
45 DOAS observations of  $HONO$  and  $NO_2$  in the Beijing area, *Atmos. Chem. Phys.*, 14, 765-781, 10.5194/acp-  
46 14-765-2014, 2014.

47 Hoesly, R. M., Smith, S. J., Feng, L., Klimont, Z., Janssens-Maenhout, G., Pitkanen, T., Seibert, J. J., Vu, L.,  
48 Andres, R. J., Bolt, R. M., Bond, T. C., Dawidowski, L., Kholod, N., Kurokawa, J.-I., Li, M., Liu, L., Lu, Z.,

1 Moura, M. C. P., O'Rourke, P. R., and Zhang, Q.: Historical (1750–2014) anthropogenic emissions of  
2 reactive gases and aerosols from the Community Emissions Data System (CEDS), *Geosci. Model Dev.*, 11,  
3 369–408, 10.5194/gmd-11-369-2018, 2018a.

4 Hoesly, R. M., Smith, S. J., Feng, L., Klimont, Z., Janssens-Maenhout, G., Pitkanen, T., Seibert, J. J., Vu, L.,  
5 Andres, R. J., Bolt, R. M., Bond, T. C., Dawidowski, L., Kholod, N., Kurokawa, J., Li, M., Liu, L., Lu, Z.,  
6 Moura, M. C. P., O'Rourke, P. R., and Zhang, Q.: Historical (1750–2014) anthropogenic emissions of  
7 reactive gases and aerosols from the Community Emissions Data System (CEDS), *Geosci. Model Dev.*, 11,  
8 369–408, 10.5194/gmd-11-369-2018, 2018b.

9 Holmes, C. D., Prather, M. J., and Vinken, G. C. M.: The climate impact of ship NO<sub>x</sub> emissions: an  
10 improved estimate accounting for plume chemistry, *Atmos. Chem. Phys.*, 14, 6801–6812, 10.5194/acp-  
11 14-6801-2014, 2014.

12 Holmes, C. D., Bertram, T. H., Confer, K. L., Graham, K. A., Ronan, A. C., Wirks, C. K., and Shah, V.: The  
13 role of clouds in the tropospheric NO<sub>x</sub> cycle: a new modeling approach for cloud chemistry and its global  
14 implications, *Geophys. Res. Lett.*, 46, GL081990, 10.1029/2019GL081990, 2019.

15 Horowitz, L. W., Fiore, A. M., Milly, G. P., Cohen, R. C., Perring, A., Wooldridge, P. J., Hess, P. G.,  
16 Emmons, L. K., and Lamarque, J.-F.: Observational constraints on the chemistry of isoprene nitrates over  
17 the eastern United States, *J. Geophys. Res.*, 112, D12S08, doi:10.1029/2006JD007747, 2007.

18 Hudman, R. C., Moore, N. E., Martin, R. V., Russell, A. R., Mebust, A. K., Valin, L. C., and Cohen, R. C.: A  
19 mechanistic model of global soil nitric oxide emissions: implementation and space based-constraints,  
20 *Atmos. Chem. Phys.*, 12, 7779–7795, 10.5194/acp-12-7779-2012, 2012.

21 Ishino, S., Hattori, S., Savarino, J., Jourdain, B., Preunkert, S., Legrand, M., Caillon, N., Barbero, A.,  
22 Kuribayashi, K., and Yoshida, N.: Seasonal variations of triple oxygen isotopic compositions of  
23 atmospheric sulfate, nitrate, and ozone at Dumont d'Urville, coastal Antarctica, *Atmos. Chem. Phys.*, 17,  
24 3713–3727, 10.5194/acp-17-3713-2017, 2017a.

25 Ishino, S., Hattori, S., Savarino, J., Jourdain, B., Preunkert, S., Legrand, M., Caillon, N., Barbero, A.,  
26 Kuribayashi, K., and Yoshida, N.: Seasonal variations of triple oxygen isotopic compositions of  
27 atmospheric sulfate, nitrate, and ozone at Dumont d'Urville, coastal Antarctica, *Atmos. Chem. Phys.*, 17,  
28 3713–3727, 10.5194/acp-17-3713-2017, 2017b.

29 Jacob, D. J.: Heterogeneous chemistry and tropospheric ozone, *Atmos. Env.*, 34, 2131–2159, 2000.

30 Jacobs, M. I., Burke, W. J., and Elrod, M. J.: Kinetics of the reactions of isoprene-derived hydroxynitrates:  
31 gas phase epoxide formation and solution phase hydrolysis, *Atmos. Chem. Phys.*, 2014, 8933–8946,  
32 10.5194/acp-14-8933-2014, 2014.

33 Jaeglé, L., Steinberger, L., Martin, R. V., and Chance, K.: Global partitioning of NO<sub>x</sub> sources using satellite  
34 observations: Relative roles of fossil fuel combustion, biomass burning and soil emissions, *Faraday  
35 Discussions*, 130, 407–423, DOI: 10.1039/b502128f, 2005.

36 Jaeglé, L., Shah, V., Thornton, J. A., Lopez-Hilfiker, F. D., Lee, B. H., McDuffie, E. E., Fibiger, D., Brown, S.,  
37 Veres, P., Sparks, T. L., Ebben, C. J., Wooldridge, P. J., Kenagy, H. S., Cohen, R. C., Weinheimer, A. J.,  
38 Campos, T. L., Montzka, D. D., Digangi, J. P., Wolfe, G. M., Hanisco, T., Schroder, J. C., Campuzano-Jost,  
39 P., Day, D. A., Jimenez, J. L., Sullivan, A. P., Guo, H., and Weber, R. J.: Nitrogen oxides emissions,  
40 chemistry, deposition, and export over the Northeast United States during the WINTER aircraft  
41 campaign, *J. Geophys. Res.*, 123, 12,368–312,393, doi.org/10.1029/2018JD029133, 2018.

42 Jenkin, M. E., Cox, R. A., and Williams, D. J.: Laboratory studies of the kinetics of formation of nitrous  
43 acid from the thermal reaction of nitrogen dioxide and water vapor, *Atm. Env.*, 22, 487–498, 1988.

44 Johnston, J. C., and Thiemens, M. H.: The isotopic composition of tropospheric ozone in three  
45 environments, *J. Geophys. Res.*, 102, 25395–25404, 1997.

46 Kaiser, J., Hastings, M. G., Houlton, B. Z., Rockmann, T., and Sigman, D. M.: Triple Oxygen Isotope  
47 Analysis of Nitrate Using the Denitrifier Method and Thermal Decomposition of N<sub>2</sub>O, *Anal. Chem.*, 79,  
48 599–607, 2007.

1 Kasibhatla, P., Sherwen, T., Evans, M. J., Carpenter, L. J., Reed, C., Alexander, B., Chen, Q., Sulprizio, M.  
2 P., Lee, J. D., Read, K. A., Bloss, W. J., Crilley, L. R., Keene, W. C., Pzenny, A. A. P., and Hodzic, H.: Global  
3 impact of nitrate photolysis of sea-salt aerosol on NO<sub>x</sub>, OH and ozone in the marine boundary layer,  
4 Atmos. Chem. Phys., 18, 11185-11203, 10.5194/acp-18-11185-2018 2018.

5 Krankowsky, D., Bartecki, F., Klees, G. G., Mauersberger, K., Schellenback, K., and Stehr, J.: Measurement  
6 of heavy isotope enrichment in tropospheric ozone, Geophys. Res. Lett., 22, 1713-1716, 1995.

7 Krankowsky, D., Lammerzahl, P., and Mauersberger, K.: Isotopic measurements of stratospheric ozone,  
8 Geophys. Res. Lett., 27, 2593-2595, 2000.

9 Kunasek, S. A., Alexander, B., Hastings, M. G., Steig, E. J., Gleason, D. J., and Jarvis, J. C.: Measurements  
10 and modeling of  $\Delta^{17}\text{O}$  of nitrate in a snowpit from Summit, Greenland, J. Geophys. Res. , 113, D24302,  
11 10.1029/2008JD010103, 2008.

12 Lee, C., Martin, R. V., van Donkelaar, A., Lee, H., Dickerson, R. R., Hains, J. C., Krotkov, N., Richter, A.,  
13 innikov, K., and Schwab, J. J.: SO<sub>2</sub> emissions and lifetimes: Estimates from inverse modeling using in situ  
14 and global, space-based (SCIAMACHY and OMI) observations, J. Geophys. Res., 116, D06304,  
15 10.1029/2010JD014758, 2011.

16 Lee, H.-M., Henze, D. K., Alexander, B., and Murray, L. T.: Investigating the sensitivity of surface-level  
17 nitrate seasonality in Antarctica to primary sources using a global model, Atm. Env., 89, 757-767,  
18 10.1016/j.atmosenv.2014.03.003, 2014.

19 Lee, J. H., and Tang, I. N.: Accommodation coefficient of gaseous NO<sub>2</sub> on water surfaces, Atm. Env., 22,  
20 1988.

21 Levy, H., Moxim, W. J., Klonecki, A. A., and Kasibhatla, P. S.: Simulated tropospheric NO<sub>x</sub>: Its evaluation,  
22 global distribution and individual source contributions, J. Geophys. Res, 104, 26,279-226,306, 1999.

23 Li, L., Duan, Z., Li, H., Zhu, C., Henkelman, G., Francisco, J. S., and Zeng, X. C.: Formation of HONO from  
24 the NH<sub>3</sub>-promoted hydrolysis  
25 of NO<sub>2</sub> dimers in the atmosphere, Proc. Natl. Acad. Sci., 115, 7236-7241, 10.1073/pnas.1807719115,  
26 2018a.

27 Li, L., Hoffmann, M. R., and Colussi, A. J.: Role of Nitrogen Dioxide in the Production of Sulfate during  
28 Chinese Haze-Aerosol Episodes, Env. Sci. & Tech., 52, 2686-2693, 10.1021/acs.est.7b05222, 2018b.

29 Li, M., Q. Zhang, J. Kurokawa, J. H. Woo, K. B. He, Z. Lu, T. Ohara, Y. Song, D. G. Streets, G. R. Carmichael,  
30 Y. F. Cheng, C. P. Hong, H. Huo, X. J. Jiang, S. C. Kang, F. Liu, H. Su, and Zheng, B.: MIX: a mosaic Asian  
31 anthropogenic emission inventory for the MICS-Asia and the HTAP projects, Atmos. Chem. Phys, 17,  
32 935-963, 10.5194/acp-17-935-2017, 2017.

33 Liang, J., Horowitz, L. W., Jacob, D. J., Wang, Y., Fiore, A. M., Logan, J. A., Gardner, G. M., and Munger, J.  
34 W.: Seasonal budgets of reactive nitrogen species and ozone over the United States, and export fluxes to  
35 the global atmosphere,, J. Geophys. Res., 103, 13435-13450,, 1998.

36 Liu, H., Jacob, D. J., Bey, I., and Yantosca, R. M.: Constraints from <sup>210</sup>Pb and <sup>7</sup>Be on wet deposition and  
37 transport in a global three-dimensional chemical tracer model driven by assimilated meteorological  
38 fields, J. Geophys. Res., 106, 12,109-112,128, 2001.

39 Long, M. S., Keene, W. C., Easter, R. C., Sander, R., Liu, X., Kerkweg, A., and Erickson, D.: Sensitivity of  
40 tropospheric chemical composition to halogen-radical chemistry using a fully coupled size-resolved  
41 multiphase chemistry-global climate system: halogen distributions, aerosol composition, and sensitivity  
42 of climate-relevant gases, Atmos. Chem. Phys, 14, 3397-3425, 10.5194/acp-14-3397-2014, 2014.

43 Lyons, J. R.: Transfer of mass-independent fractioation on ozone to other oxygen-containing molecules  
44 in the atmosphere, Geophys. Res. Lett., 28, 3231-3234, 2001.

45 Macintyre, H. L., and Evans, M. J.: Sensitivity of a global model to the uptake of N<sub>2</sub>O<sub>5</sub> by tropospheric  
46 aerosol, Atmos. Chem. Phys, 10, 7409-7401, 10.5194/acp-10-7409-2010, 2010.

1 Martin, R. V., Jacob, D. J., Yantosca, R. M., Chin, M., and Ginoux, P.: Global and regional decreases in  
2 tropospheric oxidants from photochemical effects of aerosols, *J. Geophys. Res.*, 108, 4097, doi:  
3 4010.1029/2002JD002622, 2003.

4 Mauersberger, K., Lämmenzahl, P., and Krankowsky, D.: Stratospheric Ozone Isotope Enrichments—  
5 Revisited, *Geophys. Res. Lett.*, 28, 3155-3158, 2001.

6 McCabe, J. R., Boxe, C. S., Colussi, A. J., Hoffmann, M. R., and Thiems, M. H.: Oxygen isotopic  
7 fractionation in the photochemistry of nitrate in water and ice, *J. Geophys. Res.*, 110, D15310, 2005.

8 McCabe, J. R., Savarino, J., Alexander, B., Gong, S., and Thiems, M. H.: Isotopic constraints on non-  
9 photochemical sulfate production in the Arctic winter, *Geophys. Res. Lett.*, 33, L05810,  
10 10.1029/2005GL025164, 2006.

11 McCabe, J. R., Thiems, M. H., and Savarino, J.: A record of ozone variability in South Pole Antarctic  
12 snow: Role of nitrate oxygen isotopes, *J. Geophys. Res.*, 112, D12303, doi:10.1029/2006JD007822, 2007.

13 Michalski, G., and Bhattacharya, S. K.: The role of symmetry in the mass independent isotope effect in  
14 ozone, *Proc. Natl. Acad. Sci.*, 106, 5493-5496, 2009.

15 Michalski, G., Bhattacharya, S. K., and Girsch, G.: NO<sub>x</sub> cycle and the tropospheric ozone isotope  
16 anomaly: an experimental investigation, *Atmos. Chem. Phys.*, 14, 4935-4953, 10.5194/acp-14-4935-2014,  
17 2014.

18 Michalski, G. M., Scott, Z., Kabiling, M., and Thiems, M. H.: First measurements and modeling of  $\Delta^{17}\text{O}$   
19 in atmospheric nitrate, *Geophys. Res. Lett.*, 30, 1870, doi:1810.1029/2003GL017015, 2003.

20 Morin, S., Savarino, J., Bekki, S., Gong, S., and Bottenheim, J. W.: Signature of Arctic surface ozone  
21 depletion events in the isotope anomaly ( $\Delta^{17}\text{O}$ ) of atmospheric nitrate, *Atmos. Chem. Phys.*, 6, 6255-  
22 6297, 2007.

23 Morin, S., Savarino, J., Frey, M. M., Yan, N., Bekki, S., Bottenheim, J. W., and Martins, J. M. F.: Tracing the  
24 Origin and Fate of NO<sub>x</sub> in the Arctic Atmosphere Using Stable Isotopes in Nitrate, *Science*, 322, 730-732,  
25 10.1126/science.1161910, 2008.

26 Morin, S., Savarino, J., Frey, M. M., Dominé, F., Jacobi, H.-W., Kaleschke, L., and Martins, J. M. F.:  
27 Comprehensive isotopic composition of atmospheric nitrate in the Atlantic Ocean boundary layer from  
28 65S to 79N, *J. Geophys. Res.*, 114, D05303, doi:10.1029/2008JD010696, 2009.

29 Morin, S., Sander, R., and Savarino, J.: Simulation of the diurnal variations of the oxygen isotope  
30 anomaly ( $\Delta^{17}\text{O}$ ) of reactive atmospheric species, *Atmos. Chem. Phys.*, 11, 3653-3671, doi:10.5194/acp-  
31 11-3653-2011, 2011.

32 Morton, J., Barnes, J., Schueler, B., and Mauersberger, K.: Laboratory studies of heavy ozone, *J. Geophys. Res.*, 95, 901-907, 1990.

33 Müller, J.-F., Peeters, J., and Stavrakou, T.: Fast photolysis of carbonyl nitrates from isoprene, *Atmos. Chem. Phys.*, 14, 2497-2508, 10.5194/acp-14-2497-2014, 2014.

34 Murray, L. T., Jacob, D. J., Logan, J. A., Hudman, R. C., and Koshak, W. J.: Optimized regional and  
35 interannual variability of lightning in a global chemical transport model constrained by LIS/OTD satellite  
36 data, *J. Geophys. Res.*, 117, D20307, 10.1029/2012JD017934, 2012.

37 Murray, L. T.: Lightning NO<sub>x</sub> and Impacts on Air Quality, *Curr. Pollution Rep.*, 2, 115-133,  
38 10.1007/s40726-016-0038-0, 2016.

39 Newsome, B., and Evans, M. J.: Impact of uncertainties in inorganic chemical rate constants on  
40 tropospheric composition and ozone radiative forcing, *Atmos. Chem. Phys.*, 17, 14333-14352,  
41 10.5194/acp-17-14333-2017, 2017.

42 O'Brien, J., Shepson, P., Muthuramu, K., Hao, C., Niki, H., Hastie, D., Taylor, R., and Roussel, P.:  
43 Measurements of alkyl and multifunctional organic nitrates at a rural site in Ontario, *J. Geophys. Res.*,  
44 100, 22795-22804, 1995.

1 Park, R. J., Jacob, D. J., Field, B. D., Yantosca, R. M., and Chin, M.: Natural and transboundary pollution  
2 influences on sulfate-nitrate-ammonium aerosols in the United States: implications for policy, *J.  
3 Geophys. Res.*, 109, D15204, 10.1029/2003JD004473, 2004.

4 Parrella, J. P., Jacob, D. J., Liang, Q., Zhang, Y., Mickley, L. J., Miller, B., Evans, M. J., Yang, X., Pyle, J. A.,  
5 Theys, N., and Roozendael, M. V.: Tropospheric bromine chemistry: implications for present and pre-  
6 industrial ozone and mercury, *Atmos. Chem. Phys.*, 12, 6723-6740, 10.5194/acp-12-6723-2012, 2012.

7 Paulot, F., Crounse, J. D., Kjaergaard, H. G., Kroll, J. H., Seinfeld, J. H., and Wennberg, P. O.: Isoprene  
8 photooxidation: new insights into the production of acids and organic nitrates, *Atmos. Chem. Phys.*, 9,  
9 1479-1501, 2009.

10 Ramazan, K. A., Syomin, D., and Finlayson-Pitts, B. J.: The photochemical production of HONO during the  
11 heterogeneous hydrolysis of NO<sub>2</sub>, *Phys. Chem. Chem. Phys.*, 6, 3836-3843, 10.1039/b402195a, 2004.

12 Reed, C., Evans, M. J., Crilley, L. R., Bloss, W. J., Sherwen, T., Read, K. A., Lee, J. D., and Carpenter, L.:  
13 Evidence for renoxification in the tropical marine boundary layer, *Atmos. Chem. Phys.*, 17, 4081-4092,  
14 10.5194/acp-17-4081-2017, 2017.

15 Richter, A., Borrows, J. P., Nub, H., Granier, C., and Niemier, U.: Increase in tropospheric nitrogen dioxide  
16 over China observed from space, *Nature*, 437, 129-132, 10.1038/nature04092, 2005.

17 Rindelaub, J. D., McAvey, K. M., and Shepson, P. B.: The photochemical production of organic nitrates  
18 from  $\alpha$ -pinene and loss via acid-dependent particle phase hydrolysis, *A`100tm. Env.*, 193-201,  
19 10.1016/j.atmosenv.2014.11.010, 2015.

20 Romer, P. S., Wooldridge, P. J., Crounse, J. D., Kim, M. J., Wennberg, P. O., Dibb, J. E., Scheuer, E., Blake,  
21 D. R., Meinardi, S., Brosius, A. L., Thamess, A. B., Miller, D. O., Brune, W. H., Hall, S. R., Ryerson, T. B., and  
22 Cohen, R. C.: Constraints on Aerosol Nitrate Photolysis as a Potential Source of HONO and NO<sub>x</sub>,  
23 *Environmental Science & Technology*, 52, 13738-13746, 10.1021/acs.est.8b03861, 2018.

24 Saiz-Lopez, A., Lamarque, J. F., Kinnison, D. E., Tilmes, S., Ordonez, C., Orlando, J. J., Conley, A. J., Plane,  
25 J. M. C., Mahajan, A. S., Sousa Santos, G., ATlas, E. L., Blake, D. R., Sander, S. P., Schauffler, S., Thompson,  
26 A. M., and Brasseur, G. P.: Estimating the climate significance of halogen-driven ozone loss in the  
27 tropical marine troposphere, *Atmos. Chem. Phys.*, 12, 3939-3949, 10.5194/acp-12-3939-2012, 2012.

28 Savarino, J., and Thiemens, M. H.: Analytical procedure to determine both  $\delta^{18}\text{O}$  and  $\delta^{17}\text{O}$  of H<sub>2</sub>O<sub>2</sub> in  
29 natural water and first measurements, *Atmos. Env.*, 33, 3683-3690, 1999b.

30 Savarino, J., Kaiser, J., Morin, S., Sigman, D. M., and Thiemens, M. H.: Nitrogen and oxygen isotopic  
31 constraints on the origin of atmospheric nitrate in coastal Antarctica, *Atmos. Chem. Phys.*, 7, 1925-1945,  
32 2007.

33 Savarino, J., Bhattacharya, S. K., Morin, S., Baroni, M., and Doussin, J.-F.: The NO+O<sub>3</sub> reaction: A triple  
34 oxygen isotope perspective on the reaction dynamics and atmospheric implications for the transfer of  
35 the ozone isotope anomaly, *J. Chem. Phys.*, 128, 194303, 10.1063/1.2917581, 2008.

36 Savarino, J., Morin, S., Erbland, J., Grannec, F., Patey, M., Vicars, W., Alexander, B., and Achterberg, E. P.:  
37 Isotopic composition of atmospheric nitrate in a tropical marine boundary layer, *PNAS*, published ahead  
38 of print, doi:10.1073/pnas.1216639110, 2013.

39 Schmidt, J. A., Jacob, D. J., Horowitz, H. M., Hu, L., Sherwen, T., Evans, M. J., Liang, Q., Sulieman, R. M.,  
40 Oram, D. E., Le Breton, M., Percival, C. J., Wang, S., Dix, B., and Volkamer, R.: Modeling the observed  
41 tropospheric BrO background: Importance of multiphase chemistry and implications for ozone, OH, and  
42 mercury, *J. Geophys. Res.*, 121, 11,819-811,835, 10.1002/2015JD024229, 2016.

43 Shah, V., Jaeglé, L., Thornton, J. A., Lopez-Hilfiker, F. D., Lee, B. H., Schroder, J. C., Campuzano-Jost, P.,  
44 Jimenez, J. L., Guo, H., Sullivan, A. P., Weber, R. J., Green, J. R., Fiddler, M. N., Bililign, S., Campos, T. L.,  
45 Stell, M., Weinheimer, A. J., Montzka, D. D., and Brown, S. S.: Chemical feedbacks weaken the  
46 wintertime response of particulate sulfate and nitrate to emissions reductions over the eastern United  
47 States, *Proc. Natl. Acad. Sci.*, 115, 8110-8115, 10.1073/pnas.1803295115, 2018.

1 Shao, J., Chen, Q., Wang, Y., Xie, Z., He, P., Sun, Y., Lu, X., Shah, V., Martin, R. V., Philip, S., Song, S., Zhao, Y., Zhang, L., and Alexander, B.: Heterogeneous sulfate aerosol formation mechanisms during  
2 wintertime Chinese haze events: Air quality model assessment using observations of sulfate oxygen  
3 isotopes in Beijing, *Atmos. Chem. Phys.*, 19, 6107-6123, 10.5194/acp-19-6107-2019, 2019.  
4 Sharma, H. D., Jervis, R. E., and Wing, K. Y.: Isotopic exchange reactions in nitrogen oxides, *J. Phys. Chem.*, 74, 923-933, 1970.  
5 Sherwen, T., Schmidt, J. A., Evans, M. J., Carpenter, L. J., Brobmann, K., Eastham, S. D., Jacob, D. J., Dix, B., Koenig, T. K., Sinreich, R., Ortega, I. K., Volkamer, R., Saiz-Lopez, A., Prados-Roman, C., Mahajan, A. S., and Ordonez, C.: Global impacts of tropospheric halogens (Cl, Br, I) on oxidants and composition in  
6 GEOS-Chem, *Atmos. Chem. Phys.*, 16, 12239-12271, 10.5194/acp-16-12239-2016, 2016.  
7 Sherwen, T., Evans, M. J., Sommariva, R., Hollis, L. D. J., Ball, S. M., Monks, P. S., Reed, C., Carpenter, L. J., Lee, J. D., Forster, G., Bandy, B., Reeves, C. E., and Bloss, W. J.: Effects of halogens on European air-  
8 quality, *Faraday Discuss.*, 200, 75-100, 10.1039/C7FD00026J, 2017.  
9 Singh, H. B., Herlth, D., O'Hara, D., Zahnle, K., Bradshaw, J. D., Sandholm, S. T., Talbot, R., Crutzen, P. J., and Kanakidou, M.: Relationship of Peroxyacetyl nitrate to active and total odd nitrogen at northern  
10 high latitudes: Influence of reservoir species on NO<sub>x</sub> and O<sub>3</sub>, *J. Geophys. Res.*, 97, 16,523-516,530, 1992.  
11 Sofen, E. D., Alexander, B., Steig, E. J., Thiemens, M. H., Kunasek, S. A., Amos, H. M., Schauer, A. J., Hastings, M. G., Bautista, J., Jackson, T. L., Vogel, L. E., McConnell, J. R., Pasteris, D. R., and Saltzman, E.  
12 S.: WAIS Divide ice core suggests sustained changes in the atmospheric formation pathways of sulfate  
13 and nitrate since the 19th century in the extratropical Southern Hemisphere, *Atmos. Chem. Phys.*, 14,  
14 5749-5769, 10.5194/acp-14-5749-2014, 2014.  
15 Spataro, F., and Ianniello, A.: Sources of atmospheric nitrous acid: State of the science, current research  
16 needs, and future prospects, *Journal of the Air and Waste Management Association*, 64, 1232-1250,  
17 10.1080/10962247.2014.952846, 2014.  
18 Stettler, M. E. J., Eastham, S., and Barrett, S. R. H.: Air quality and public health impacts of UK airports.  
19 Part I: Emissions, *Atm. Env.*, 45, 5415-5424, 10.1016/j.atmosenv.2011.07.012, 2011.  
20 Tan, F., Tong, S., Jing, B., Hou, S., Liu, Q., Li, K., Zhang, Y., and Ge, M.: Heterogeneous reactions of NO<sub>2</sub>  
21 with CaCO<sub>3</sub>-(NH<sub>4</sub>)<sub>2</sub>SO<sub>4</sub> mixtures at different relative humidities, *Atmos. Chem. Phys.*, 16, 8081-8093,  
22 10.5194/acp-16-8081-2016, 2016.  
23 Thiemens, M. H., T. Jackson: Pressure dependency for heavy isotope enhancement in ozone formation,  
24 *Geophys. Res. Lett.*, 17, 717-719, 1990.  
25 Tong, S. R., Hou, S. Q., Zhang, Y., Chu, B. W., Liu, Y. C., He, H., Zhao, P. S., and Ge, M. F.: Exploring the  
26 nitrous acid (HONO) formation mechanism in winter Beijing: direct emissions and heterogeneous  
27 production in urban and suburban areas, *Faraday Discuss.*, 189, 213-230, 10.1039/c5fd00163c, 2016.  
28 Vicars, W., and Savarino, J.: Quantitative constraints on the <sup>17</sup>O-excess ( $\Delta^{17}\text{O}$ ) signature of surface  
29 ozone: Ambient measurements from 50°N to 50°S using the nitrite-coated filter technique, *Geochem. Cosmochim. Acta*, 135, 270-287, 10.1016/j.gca.2014.03.023, 2014.  
30 Vicars, W. C., Bhattacharya, S. K., Erbland, J., and Savarino, J.: Measurement of the 17O-excess ( $\Delta^{17}\text{O}$ ) of  
31 tropospheric ozone using a nitrite-coated filter, *Rapid Commun. Mass Spectrom.*, 26, 1219-1231,  
32 10.1002/rcm.6218, 2012.  
33 Vinken, G. C. M., Boersma, K. F., Jacob, D. J., and Meijer, E. W.: Accounting for non-linear chemistry of  
34 ship plumes in the GEOS-Chem global chemistry transport model, *Atmos. Chem. Phys.*, 11, 11707-11722,  
35 10.5194/acp-11-11707-2011, 2011.  
36 von Glasow, R., and Crutzen, P. J.: Model study of multiphase DMS oxidation with a focus on halogens,  
37 *Atmos. Chem. Phys.*, 4, 589-608, 2004.  
38 Wang, F., Michalski, G., Seo, J., and Ge, W.: Geochemical, isotopic, and mineralogical constraints on  
39 atmospheric deposition in the hyper-arid Atacama Desert, Chile, *Geochem. Cosmochim. Acta*, 135, 29-  
40 48, 10.1016/j.gca.2014.03.017, 2014.

1 Wang, J. Q., Zhang, X. S., Guo, J., Wang, Z. W., and Zhang, M. G.: Observation of nitrous acid (HONO) in  
2 Beijing, China: Seasonal variation, nocturnal formation and daytime budget, *Science of the Total*  
3 *Environment*, 587, 10.1016/j.scitotenv.2017.02.159, 2017.

4 Wang, X., Jacob, D. J., Eastham, S., Sulprizio, M., Zhu, L., Chen, Q., Alexander, B., Sherwen, T., Evans, M.  
5 J., Lee, B. H., Haskins, J., Lopez-Hilfiker, F. D., Thornton, J. A., Huey, L. G., and Liao, H.: The role of  
6 chlorine in tropospheric chemistry, *Atmos. Chem. Phys. Discuss.*, 10.5194/acp-2018-1088, 2018.

7 Wang, Y. H., Jacob, D. J., and Logan, J. A.: Global simulation of tropospheric O<sub>3</sub>-NO<sub>x</sub> hydrocarbon  
8 chemistry 1. Model formulation, *J. Geophys. Res.*, 103, 10,713-710,725, 1998.

9 Xu, L., Guo, H., Boyd, C. M., Klein, M., Bougiatioti, A., Cerully, K. M., Hite, J. R., Isaacman-VanWertz, G.,  
10 Kreisberg, N. M., Knote, C., Olson, K., Koss, A., Goldstein, A. H., Hering, S. V., de Gouw, J., Baumann, K.,  
11 Lee, S.-H., Nenes, A., Weber, R. J., and Ng, N. L.: Effects of anthropogenic emissions on aerosol formation  
12 from isoprene and monoterpenes in the southeastern United States, *Proc. Natl. Acad. Sci.*, 112, 37–42,  
13 10.1073/pnas.1417609112, 2015.

14 Xu, W., Kuang, Y., Zhao, C., Tao, J., Zhao, G., Bian, Y., Yu, Y., Shen, C., Liang, L., and Zhang, G.: NH<sub>3</sub>-  
15 promoted hydrolysis of NO<sub>2</sub> induces explosive 1 growth in HONO, *Atmos. Chem. Phys. Discuss.*,  
16 <https://doi.org/10.5194/acp-2018-996>, 2018.

17 Yabushita, A., Enami, S., Sakamoto, Y., Kawasaki, M., Hoffman, M. R., and Colussi, A. J.: Anion-Catalyzed  
18 Dissolution of NO<sub>2</sub> on Aqueous Microdroplets, *J. Phys. Chem. A Lett.*, 113, 4844–4848,  
19 10.1021/jp900685f, 2009.

20 Yang, X., Cox, R. A., Warwick, N. J., Pyle, J. A., Carver, G. C., O'Connor, F. M., and Savage, N. H.:  
21 Tropospheric bromine chemistry and its impact on ozone: A model study, *J. Geophys. Res.*, 110, D2331,  
22 doi:10.1029/2005JD003244, 2005.

23 Ye, C., Zhou, X., Pu, D., Stutz, J., Festa, J., Spolaor, M., Tsai, C., Cantrell, C., Mauldin III, R. L., Campos, T.,  
24 Weinheimer, A., Hornbrook, R. S., Apel, E., Guenther, A., Kaser, L., Yuan, B., Karl, T., Haggerty, J., Hall, S.,  
25 Ullmann, K., Smith, J. N., Ortega, J., and Knote, C.: Rapid cycling of reactive nitrogen in the marine  
26 boundary layer, *Nature*, 532, 489-491, 10.1038/nature17195, 2016.

27 Ye, C., Zhou, X., Pu, D., Stutz, J., Festa, J., Spolaor, M., Tsai, C., Cantrell, C., Mauldin III, R. L., Weinheimer,  
28 A., Hornbrook, R. S., Apel, E. C., Guenther, A., Kaser, L., Yuan, B., Karl, T., Haggerty, J., Hall, S., Ullmann,  
29 K., Smith, J., and Ortega, J.: Tropospheric HONO distribution and chemistry in the southeastern US,  
30 *Atmos. Chem. Phys.*, 18, 9107-9120, 10.5194/acp-18-9107-2018, 2018.

31 Zare, A., Romer, P. S., Nguyen, T., Keutsch, F. N., Skog, K., and Cohen, R. C.: A comprehensive organic  
32 nitrate chemistry: insights into the lifetime of atmospheric organic nitrates, *Atmos. Chem. Phys.*  
33 *Discuss.*, 10.5194/acp-2018-530, 2018.

34 Zhang, L., Gong, S., Padro, J., and Barrie, L.: A size-segregated particle dry deposition scheme for an  
35 atmospheric aerosol module, *Atmos. Env.*, 35, 549-560, 2001.

36

37

38

39

40

41

1 **Table 1.** Calculated  $\Delta^{17}\text{O}$ (nitrate) in the model for each nitrate production pathway (X = Br, Cl,  
2 and I; HC = hydrocarbon; MTN = monoterpane; ISOP = isoprene;  $\Delta^{17}\text{O}(\text{O}_3^*) = 39\text{\textperthousand}$ ). A is  
3 defined in equation E1.

4

	Nitrate formation pathway	$\Delta^{17}\text{O}(\text{nitrate})$
Gas-phase reactions		
R1	$\text{NO}_2 + \text{OH}$	$\frac{2}{3} A \Delta^{17}\text{O}(\text{O}_3^*)$
R2	$\text{NO}_3 + \text{HC}$	$(\frac{2}{3} A + \frac{1}{3}) \Delta^{17}\text{O}(\text{O}_3^*)$
R3	$\text{NO} + \text{HO}_2$	$\frac{1}{3} A \Delta^{17}\text{O}(\text{O}_3^*)$
Aerosol uptake from the gas-phase followed by hydrolysis		
R4	$\text{N}_2\text{O}_5 + \text{H}_2\text{O}_{(\text{aq})}$	$(\frac{2}{3} A + \frac{1}{6}) \Delta^{17}\text{O}(\text{O}_3^*)$
R5	$\text{N}_2\text{O}_5 + \text{Cl}^-(\text{aq})$	$(\frac{2}{3} A + \frac{1}{3}) \Delta^{17}\text{O}(\text{O}_3^*)$
R6	$\text{XNO}_3 + \text{H}_2\text{O}_{(\text{aq})}$	$(\frac{2}{3} A + \frac{1}{3}) \Delta^{17}\text{O}(\text{O}_3^*)$
R7	$\text{NO}_2 + \text{H}_2\text{O}_{(\text{aq})}$	$\frac{2}{3} A \Delta^{17}\text{O}(\text{O}_3^*)$
R8	$\text{NO}_3 + \text{H}_2\text{O}_{(\text{aq})}$	$(\frac{2}{3} A + \frac{1}{3}) \Delta^{17}\text{O}(\text{O}_3^*)$
R9	$\text{RONO}_2 + \text{H}_2\text{O}_{(\text{aq})}$ (where $\text{RONO}_2$ is from $\text{NO} + \text{RO}_2$ )	$\frac{1}{3} A \Delta^{17}\text{O}(\text{O}_3^*)$
R10	$\text{RONO}_2 + \text{H}_2\text{O}_{(\text{aq})}$ (where $\text{RONO}_2$ is from $\text{NO}_3 + \text{MTN/ISOP}$ )	$(\frac{2}{3} A + \frac{1}{3}) \Delta^{17}\text{O}(\text{O}_3^*)$

5

6

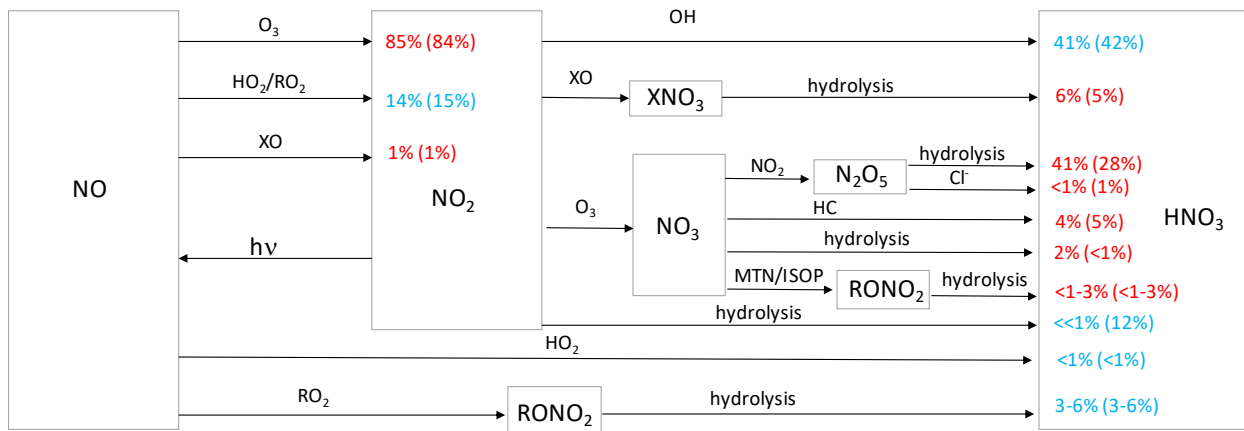
7

8

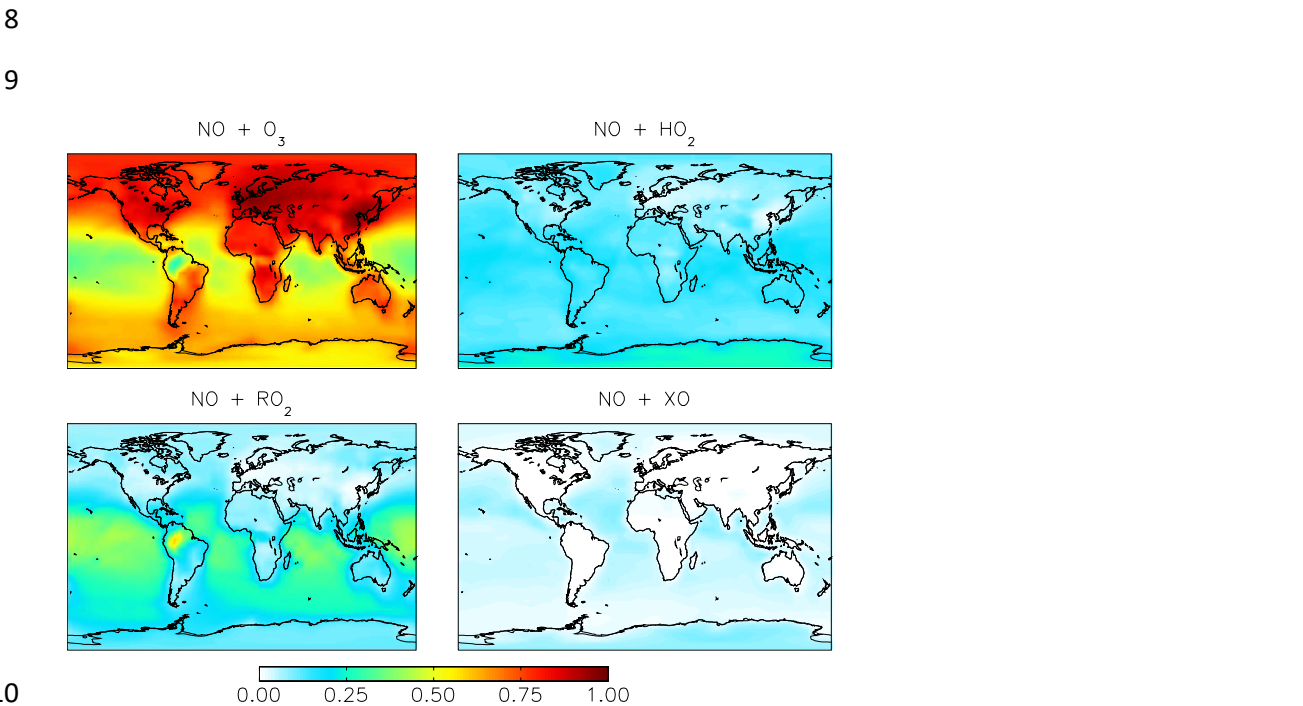
9

10

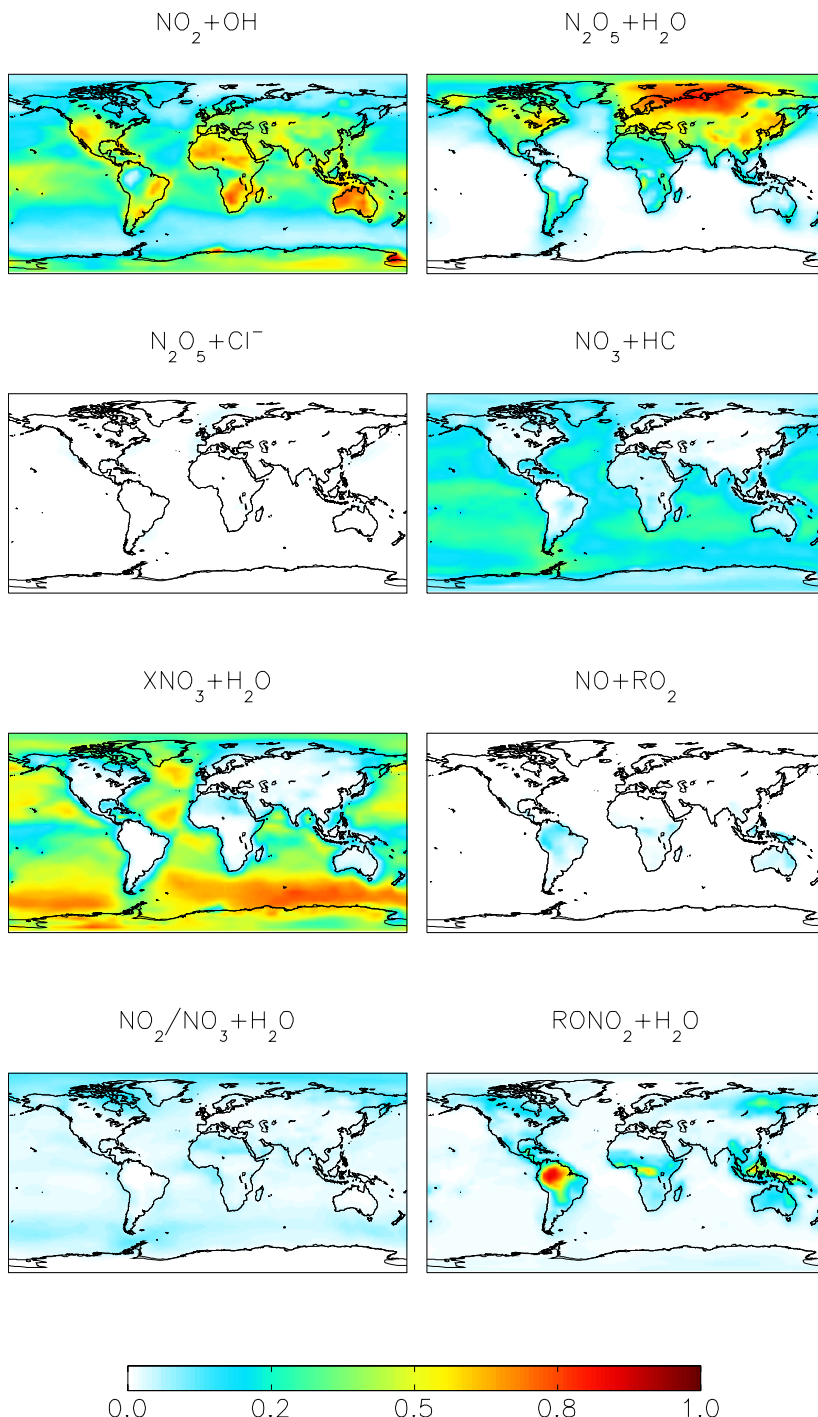
11



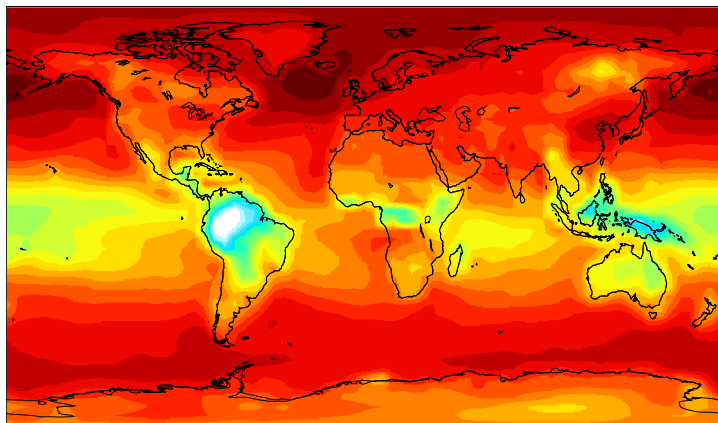
1 **Figure 1.** Simplified HNO<sub>3</sub> formation in the model. Numbers show the global, annual mean percent  
 2 contribution to NO<sub>2</sub> and HNO<sub>3</sub> formation in the troposphere below 1 km for the “cloud chem”  
 3 (“standard”) simulation. Red indicates reactions leading to high  $\Delta^{17}\text{O}$  values, blue indicates reactions  
 4 leading to low  $\Delta^{17}\text{O}$  values. HO<sub>2</sub> = HO<sub>2</sub>+RO<sub>2</sub>; X = Br+Cl+I; HC = hydrocarbons; MTN = monoterpenes;  
 5 ISOP = isoprene.



10 **Figure 2.** Annual-mean fraction of NO<sub>2</sub> formation from the oxidation of NO in the troposphere below 1  
 11 km altitude in the “cloud chemistry” model.



2 **Figure 3.** Annual-mean fraction of  $\text{HNO}_3$  formation from the oxidation of  $\text{NO}_x$  in the troposphere below 1  
3 km altitude in the "cloud chemistry" model.



2

3 **Figure 4.** Modeled, annual-mean  $\Delta^{17}\text{O}(\text{nitrate})$  below 1 km altitude for the “cloud chemistry” model.

4

5

6

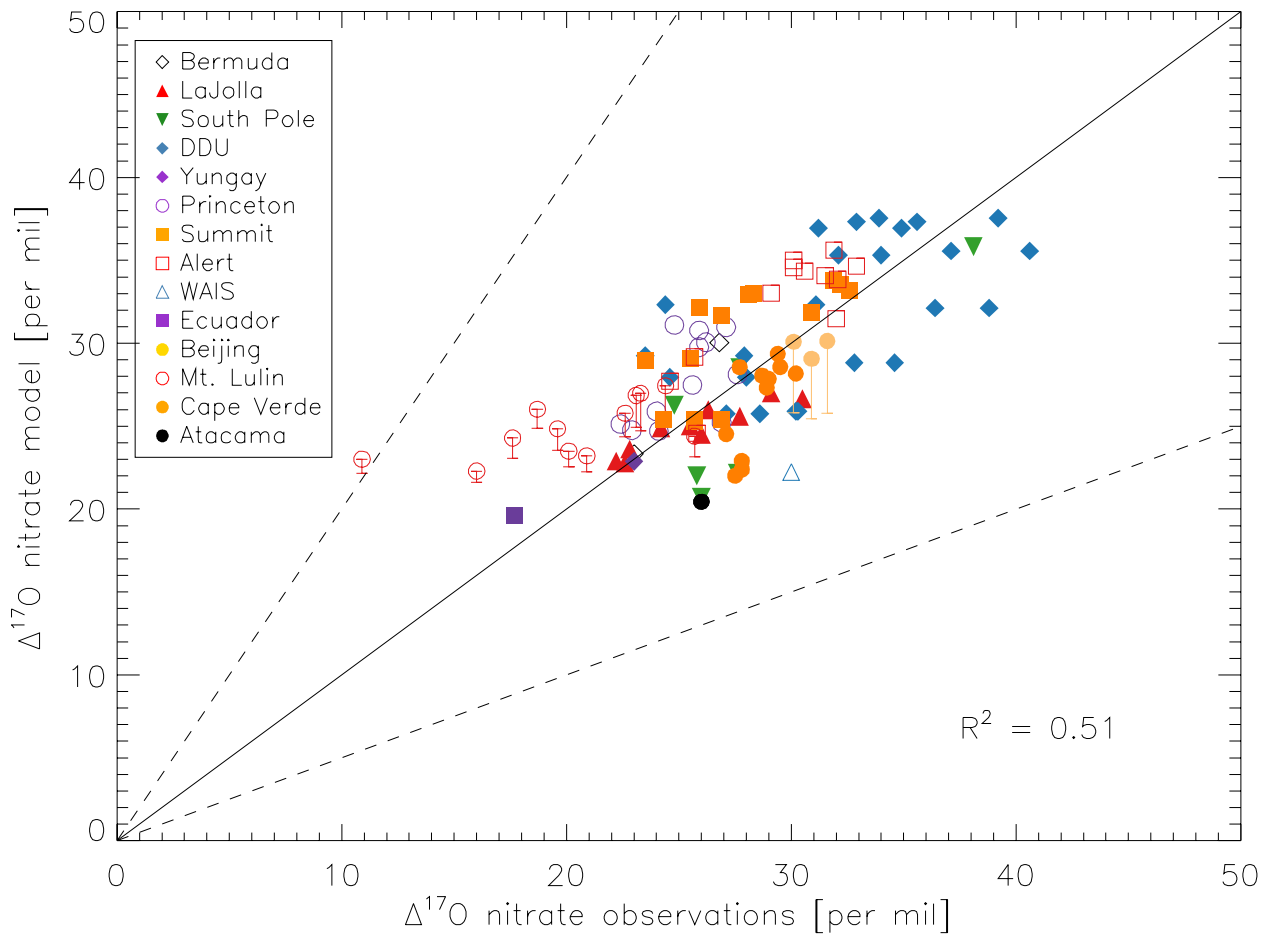
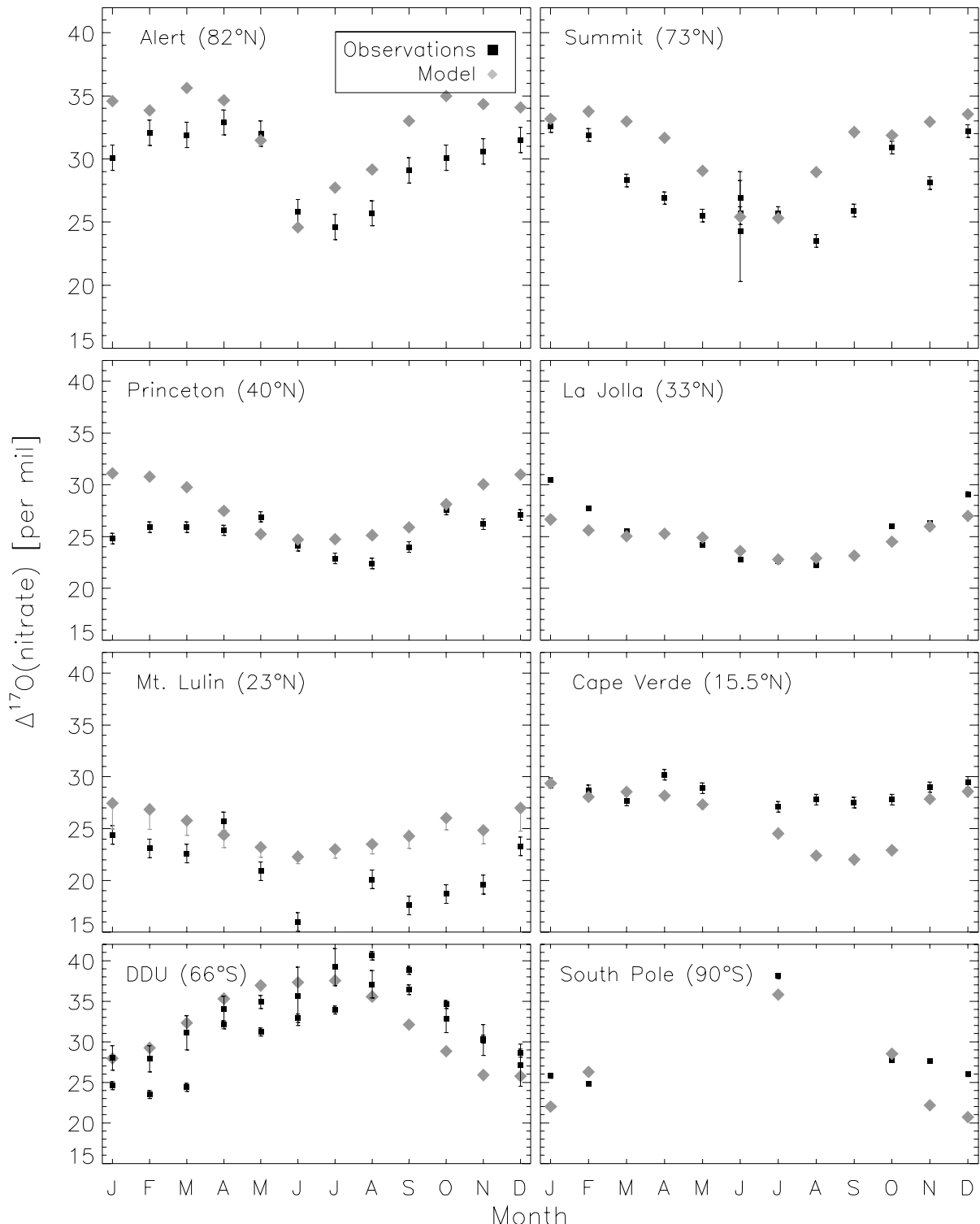


**Figure 5.** Comparison of monthly-mean modeled (“cloud chemistry”) and observed  $\Delta^{17}\text{O}(\text{nitrate})$  at locations where there are enough observations to calculate a monthly mean. References for the observations are in the text. The error bars represent different assumptions for calculated modeled  $A$  values for nighttime reactions as described in the text. Error bars for Beijing and Mt. Lulin reflect the range of possible modeled  $A$  values for nighttime reactions as described in the text. The  $y=x$  (solid line) and  $y = 2x$  and  $y = 0.5x$  (dashed) are shown.



1  
2 **Figure 6.** Comparison of monthly-mean modeled (“cloud chemistry”) and observed  $\Delta^{17}\text{O}(\text{nitrate})$ . Error  
3 bars for model results from Mt. Lulin reflect the range of possible modeled  $A$  values for nighttime  
4 reactions as described in the text. Error bars for the observations reflect the analytical uncertainty in the  
5 measurements, except for two data points in June for Summit which reflect the standard deviation of  
6  $\Delta^{17}\text{O}(\text{nitrate})$  from multiple measurements during that month.

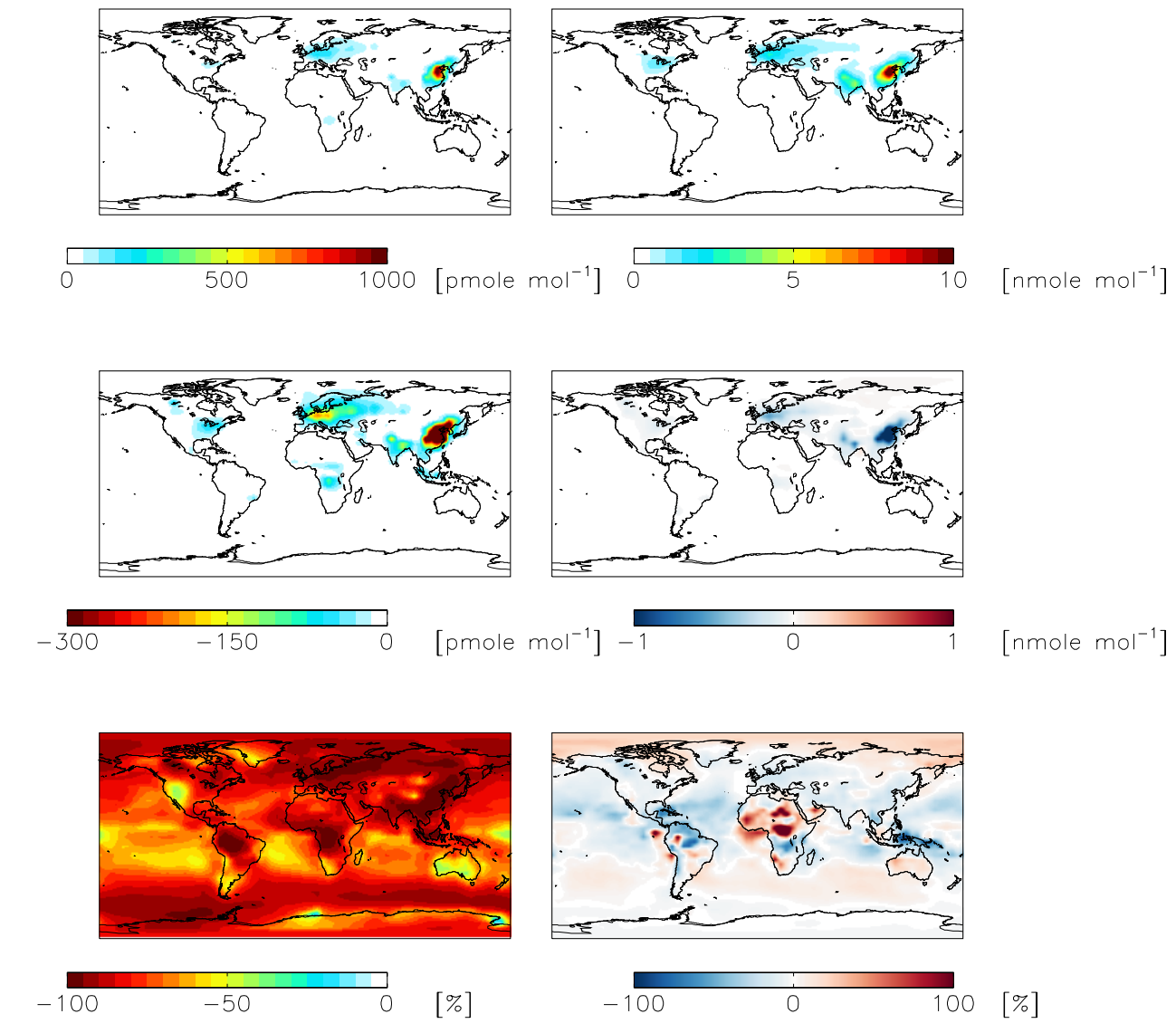
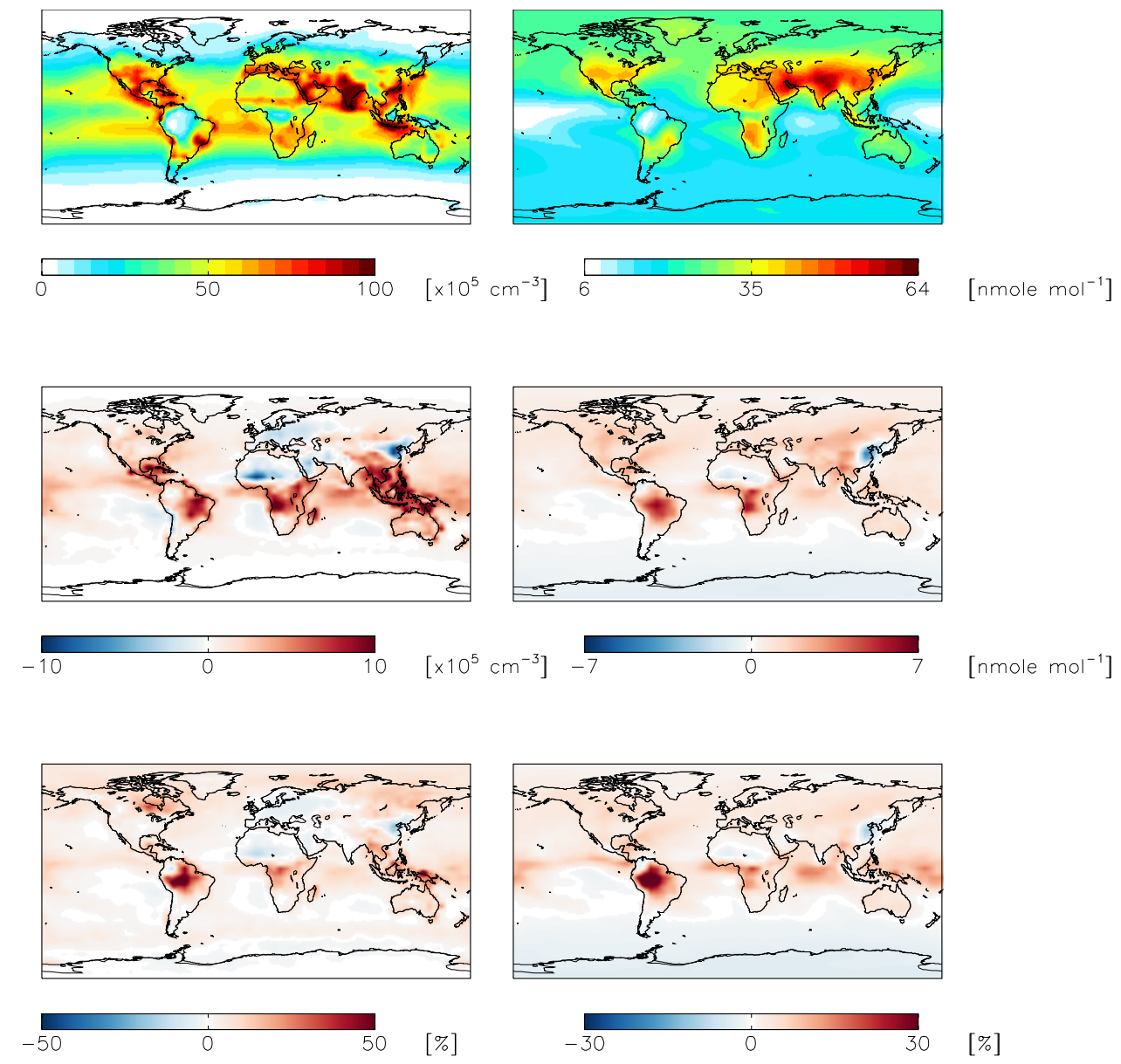


**Figure 7.** Modeled annual-mean HONO (left) and fine-mode nitrate (right) concentrations below 1 km altitude in the “standard” simulation (top) with  $\gamma_{\text{NO}_2} = 10^{-4}$  for  $\text{NO}_2$  hydrolysis. Absolute (middle) and relative (bottom) change in concentrations below 1 km altitude between the “standard” model and the model simulation with  $\gamma_{\text{NO}_2} = 10^{-7}$ . Negative numbers represent a decrease relative to the standard simulation.



2 **Figure 8.** Same as Figure 7 except for OH (left) and ozone (right).

3

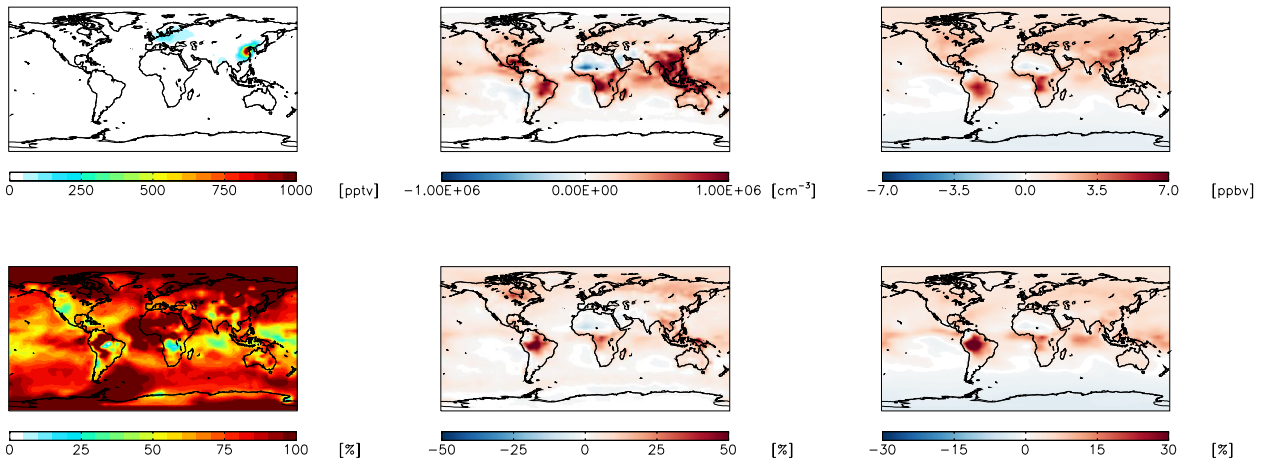


Figure 9. Absolute (top) and relative (bottom) change in HONO (left), OH (middle), and ozone (right) concentrations below 1 km altitude between the “standard” model and the model simulation with an acidity-dependent yield from  $\text{NO}_2$  hydrolysis. Positive numbers represent an increase relative to the “standard” simulation.

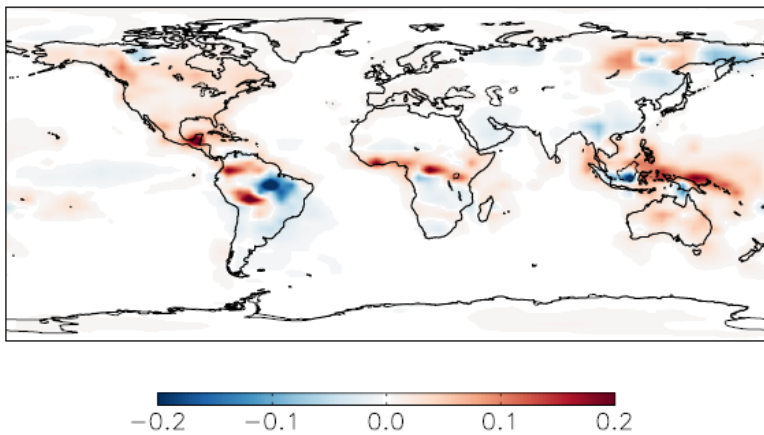


Figure 10. Modeled annual-mean difference in the fractional production rate of  $\text{HNO}_3$  from the hydrolysis of organic nitrate below 1 km altitude in the year 2015 relative to 2000 (2015 – 2000).